



Emission solvatochromic, solid-state and aggregation-induced emissive α -pyrones and emission-tuneable 1*H*-pyridines by Michael addition–cyclocondensation sequences

Natascha Breuer¹, Irina Gruber², Christoph Janiak² and Thomas J. J. Müller^{*1}

Full Research Paper

Open Access

Address:

¹Heinrich-Heine Universität Düsseldorf, Institut für Organische Chemie und Makromolekulare Chemie, Universitätsstraße 1, D-40225 Düsseldorf, Germany and ²Heinrich-Heine Universität Düsseldorf, Institut für Anorganische Chemie und Strukturchemie, Universitätsstraße 1, D-40225 Düsseldorf, Germany

Email:

Thomas J. J. Müller* - ThomasJJ.Mueller@uni-duesseldorf.de

* Corresponding author

Keywords:

cyclocondensation; DFT calculations; fluorescence; heterocycles; 1*H*-pyridines; α -pyrones

Beilstein J. Org. Chem. **2019**, *15*, 2684–2703.

doi:10.3762/bjoc.15.262

Received: 16 July 2019

Accepted: 24 October 2019

Published: 12 November 2019

This article is part of the thematic issue "Dyes in modern organic chemistry".

Guest Editor: H. Ihmels

© 2019 Breuer et al.; licensee Beilstein-Institut.

License and terms: see end of document.

Abstract

Starting from substituted alkynes, α -pyrones and/or 1*H*-pyridines were generated in a Michael addition–cyclocondensation with ethyl cyanoacetate. The peculiar product formation depends on the reaction conditions as well as on the electronic substitution pattern of the alkyne. While electron-donating groups furnish α -pyrones as main products, electron-withdrawing groups predominantly give the corresponding 1*H*-pyridines. Both heterocycle classes fluoresce in solution and in the solid state. In particular, dimethylamino-substituted α -pyrones, as donor–acceptor systems, display remarkable photophysical properties, such as strongly red-shifted absorption and emission maxima with daylight fluorescence and fluorescence quantum yields up to 99% in solution and around 11% in the solid state, as well as pronounced emission solvatochromism. Also a donor-substituted α -pyrone shows pronounced aggregation-induced emission enhancement.

Introduction

A high sensitivity and precise tuneability of fluorescence colors are prerequisites for the application of fluorescent substances in chemistry, medicine and materials science [1]. With this respect emissive small molecules [2], fluorescent proteins [3], and quantum dots have received considerable attention and remarkable progress in their synthesis and photophysics has been

achieved [4]. Small molecule organic fluorophores are particularly advantageous due to the potential of a tailored fine-tuning of their photophysical properties through synthetic modifications [5]. Based on their structural features, functionalized organic chromophores, containing N-, O- or S-atoms, are increasingly used in OLEDs [6-10] and LCDs [11-13] of mobile

phones [14]. Fluorescent compounds often intensively emit in solution but only weakly or not in the solid state [15]. Dyes which fluoresce both in the solid state and in solution are still relatively rare, due to the fact that often molecular aggregation in the solid state causes fluorescence quenching [16].

In recent years, we have coined diversity-oriented syntheses of functional chromophores by multicomponent strategies [17,18], opening accesses to substance libraries for systematic studies of structure–property relationships on fluorophores [19], in particular on aggregation-induced emissive polar dyes [20]. Conceptually, many of these consecutive multicomponent syntheses rely on transition-metal-catalyzed heterocyclic syntheses [21]. By virtue of catalytic generation of alkynes [22] we have recently disclosed consecutive alkynylation–Michael addition–cyclocondensation (AMAC) multicomponent syntheses of α -pyrones [23].

While most α -pyrones neither fluoresce in solution nor in the solid state specific substitution patterns have been identified for fluorophore design for this heterocyclic family. Tominaga and co-workers synthesized a series of α -pyrone derivatives with emission maxima between 400 and 675 nm in the solid state and between 486 and 542 nm in chloroform [16,24–26], including fluorescence quantum yields as high as 95% in solution and 58% in the solid state [16,24]. While these fluorophores were synthesized by cyclocondensation with ketene dithioacetals and substituted acetophenones other cyano-containing derivatives became accessible by desymmetrizing cyclocondensation of

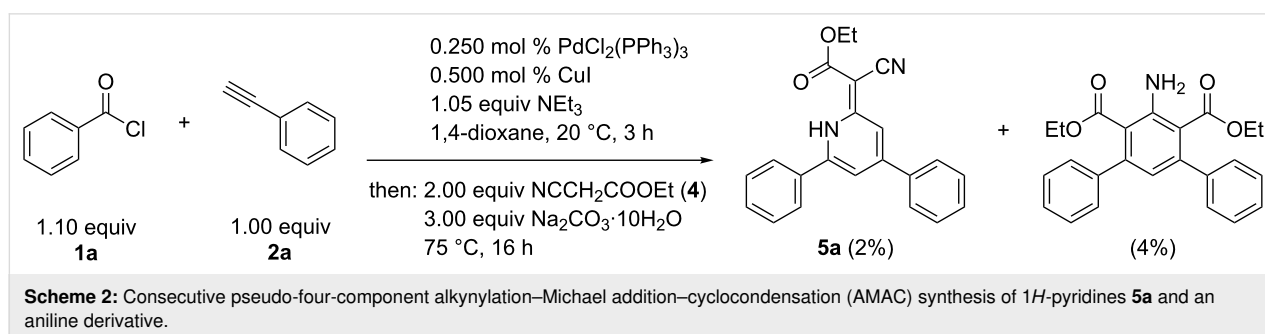
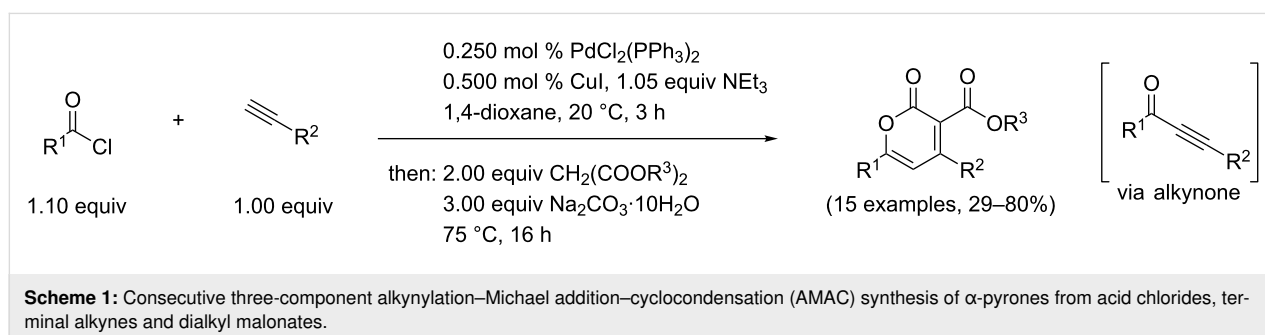
1,2-diaroylacetylenes with ethyl cyanoacetate [27], similar to related studies with dialkyl malonates [28]. Here, we report on effects of base and temperature on Michael addition–cyclocondensation sequences in the formation of α -pyrones and/or 1*H*-pyridines starting from diversely substituted alkynones and cyanoethylacetate. This bifurcating domino process furnishes small chromophore libraries which were characterized by photophysical studies (absorption and emission spectroscopy) and the studies on the electronic structure were accompanied by TD-DFT calculations for assigning the dominant longest-wavelength absorption bands.

Results and Discussion

Synthesis and tentative mechanism

Recently, we reported a straightforward access to α -pyrones through a consecutive alkynylation–Michael addition–cyclocondensation (AMAC) multicomponent synthesis [23]. The reaction can be rationalized by a Sonogashira coupling between an acid chloride and a terminal alkyne furnishing an alkynone, which is transformed without isolation by addition of dialkyl malonates in a Michael addition–cyclocondensation to form α -pyrones (Scheme 1).

With this sequence in hand, we envisioned the variation of CH-acidic esters to generate differently 3-substituted α -pyrones. For introducing a cyano substituent we employed benzoyl chloride (**1a**), phenylacetylene (**2a**), and ethyl cyanoacetate (**4**) within the AMAC sequence (Scheme 2). Surprisingly, the desired α -pyrone was not isolated, but two other compounds



were detected. On the one hand a 1*H*-pyridine derivative **5a** (2% yield) and on the other hand an aniline derivative with two ester groups (4% yield). Both compounds indicate that two molecules of ethyl cyanoacetate (**4**) were incorporated in the final structure.

With an increased amount of ethyl cyanoacetate the yield of both products could be increased. By the addition of ethanol as a cosolvent in the second step of the sequence, 1*H*-pyridine **5a** could be isolated in 30% yield, while the aniline derivative was not formed (Scheme 3).

There are only a few known methods for the synthesis of this kind of 1*H*-pyridines. In a cyclocondensation, starting from 1,3-dicarbonyl compounds, Elnagdi and co-workers synthesized 1*H*-pyridines with an additional cyano substituent in the 3-position [29]. Most syntheses generating 1*H*-pyridines make use of ethyl cyanoacetate as a starting material. It can react with itself and forms a dimer by selfcondensation, catalyzed by transition metals [30,31].

Intrigued by the unusual pseudo-four-component AMAC synthesis we investigated the reaction conditions of the terminal Michael addition–cyclocondensation step starting from alkynone **3a**. By varying the amount of the base we could observe the formation of 1*H*-pyridine **5a**, but also of α -pyrone **6a** (Scheme 4, Table 1), similarly to the reaction of compound **4** with 1,2-diaroylacetylenes [28].

Table 1: Optimization of the cyclization step of 1,5-diacyl-5-hydroxypyrazoline **5b**.^a

Entry	Base (equiv)	Compound 5a (yield) ^b	Compound 6a (yield) ^b
1	Na ₂ CO ₃ ·10H ₂ O (0.80)	20%	50%
2	Na ₂ CO ₃ ·10H ₂ O (1.0)	8%	64%
3	Na ₂ CO ₃ ·10H ₂ O (1.5)	32%	–
4	Na ₂ CO ₃ ·10H ₂ O (2.0)	26%	–
5	Na ₂ CO ₃ (0.80)	3%	41%
6 ^c	Na ₂ CO ₃ (0.80)	22%	52%
7 ^b	Na ₂ CO ₃ (1.4)	9%	66%

^aAll reactions were carried out on a 0.500 mmol scale (c₀(**3a**) = 0.50 M, c₀(**4**) = 2.0 M; ^ball yields refer to isolated and purified products; ^cadditional water (5.6 equiv).

With either 0.8 or 1.0 equiv of Na₂CO₃·10H₂O α -pyrone **6a** is formed as the main product (50–64%), while 1*H*-pyridine **5a** can also be isolated in around 15% yield (Table 1, entries 1 and 2). By increasing the amount of Na₂CO₃·10H₂O, exclusively 1*H*-pyridine **5a** can be isolated in low yield (Table 1, entries 3 and 4). Using anhydrous sodium carbonate α -pyrone **6a** is again formed as the main product in 41% yield, but the yield of 1*H*-pyridine **5a** drops to 3% (Table 1, entry 5). By the addition of water, the yield of **6a** could be increased (Table 1, entries 6 and 7).

Next we evaluated the use of a mixture of two bases, sodium carbonate and sodium acetate, and water (Table 2). With

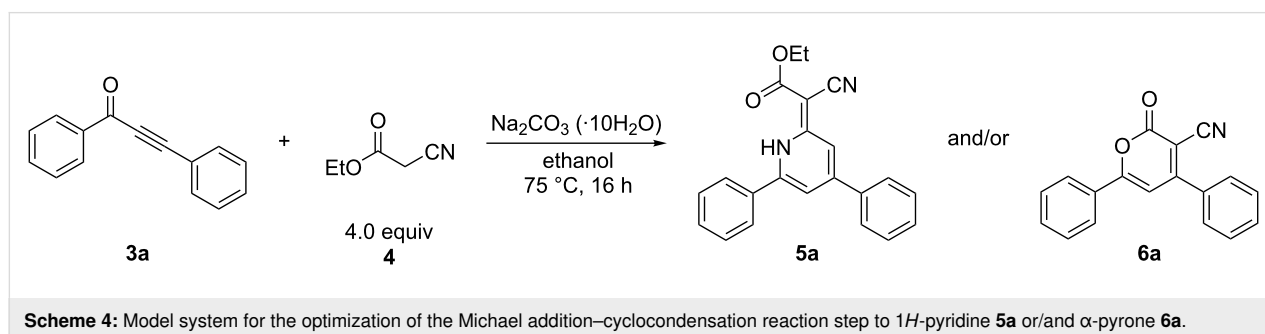
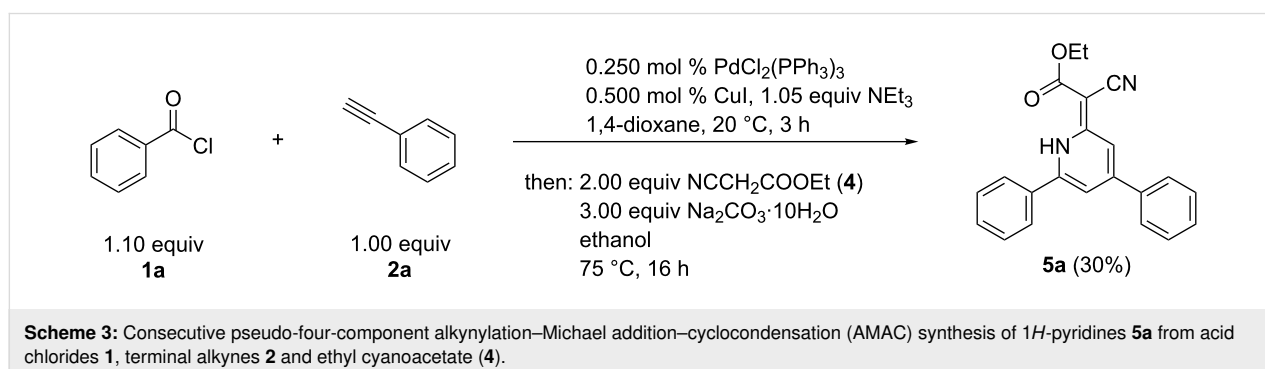


Table 2: Optimization of the formation of 1*H*-pyridine **5a** or/and α -pyrone **6a** in the Michael addition–cyclocondensation reaction with Na₂CO₃, NaOAc and water.^a

Entry	Na ₂ CO ₃ [equiv]	NaOAc [equiv]	H ₂ O [equiv]	Compound 5a (yield) ^b	Compound 6a (yield) ^b
1	0.80	0.60	5.6	56%	–
2 ^c	0.80	0.60	5.6	26%	–
3 ^d	0.80	0.60	5.6	56%	–
4	0.80	0.60	–	44%	–
5	–	0.60	–	26%	28%
6	–	0.60	5.6	23%	–
7	0.80	0.60	2.8	40%	–
8	0.80	0.60	8.4	40%	20%
9	0.80	0.60	11	38%	28%
10	1.0	0.60	5.6	45%	–
11	0.80	0.80	5.6	43%	–

^aAll reactions were carried out on a 0.500 mmol scale (*c*₀(**3a**) = 0.50 M, *c*₀(**4**) = 2.0 M; ^ball yields refer to isolated and purified products; ^c*c*₀(**4**) = 1.0 M; ^dadditional 4.0 equiv of ethyl cyanoacetate (**4**) after 2 h.

0.80 equiv of sodium carbonate, 0.60 equiv of sodium acetate and 5.6 equiv of water 1*H*-pyridine **5a** could be isolated in 56% yield. Decreasing the amount of ethyl cyanoacetate (**4**) the yields drops (Table 2, entry 2), however, increasing the amount of substrate **4** does not improve the yield (Table 2, entry 3). The exclusion of water only causes a decrease in yield (Table 2, entry 4). With sodium acetate as the only base, both 1*H*-pyridine **5a** and α -pyrone **6a** are formed in ca. 25% yield each (Table 2, entry 5). Sodium acetate with additional water gives

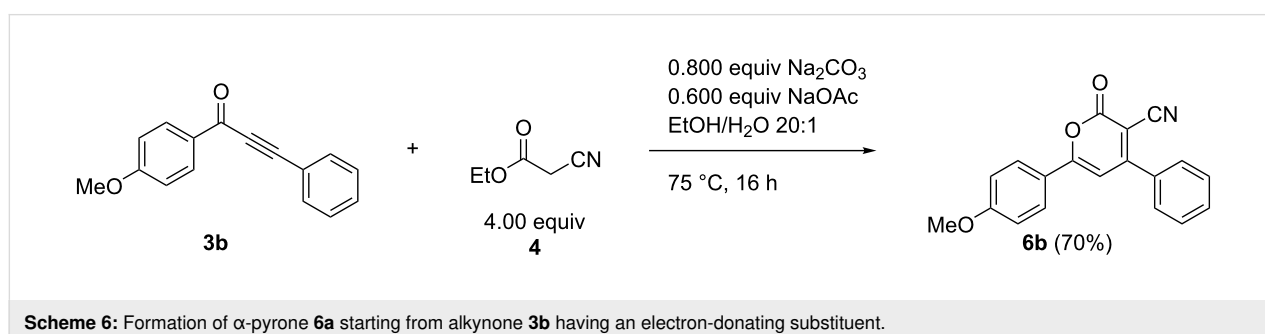
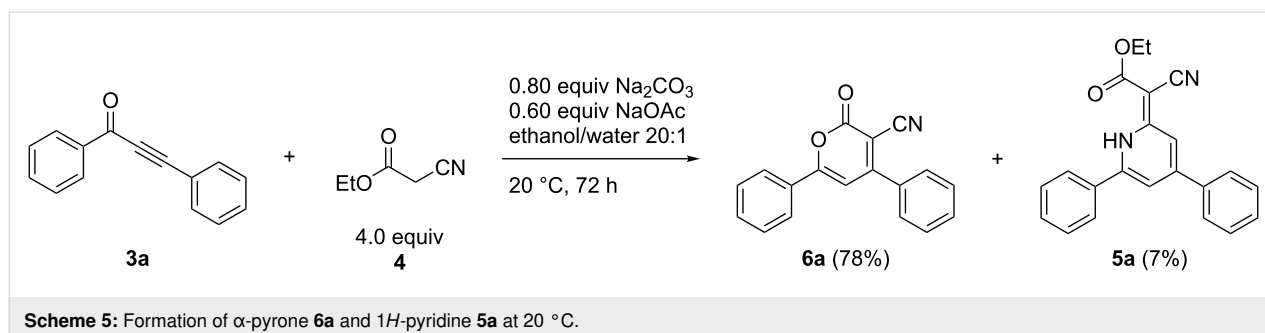
1*H*-pyridine **5a** in 23% yield (Table 2, entry 6). It seems to be important that both bases and water are present, but neither a reduction nor an increase of the amount of water increased the yields of 1*H*-pyridine **5a** (Table 2, entries 7–9). The increase of neither sodium carbonate (Table 2, entry 10) nor sodium acetate (Table 2, entry 11) caused an increase in yields.

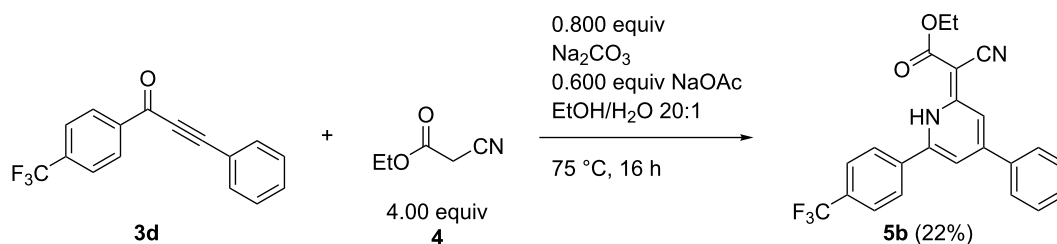
Only lowering the reaction temperature to 20 °C α -pyrone **6a** was isolated as the main product in 78% yield and 1*H*-pyridine **5a** was obtained in only 7% yield (Scheme 5).

Since base(s) and reaction temperature exert a significant impact on which heterocyclic compound is formed, we also tried to change the electronic nature of the starting material. Therefore, an electron-donating substituent was introduced in the alkynone **3b** and the reaction was performed at 75 °C. To our surprise, we only could isolate α -pyrone **6b** (Scheme 6).

However, when we introduced an electron-withdrawing group 1*H*-pyridine **5b** was the only product (Scheme 7).

For elucidating whether 1*H*-pyridine **5a** is formed from α -pyrone **6a** and ethyl cyanoacetate (**4**) a reaction between α -pyrone **6a** and ethyl cyanoacetate (**4**) under the same reaction conditions as for the 1*H*-pyridine from alkynone **3a** was conducted, but only starting material could be isolated. Another option for the formation of the 1*H*-pyridine **5a** was envisioned by an in situ generation of a dimer of ethyl cyanoacetate (**4**). The dimer **7** can be synthesized by iridium catalysis [30]. With



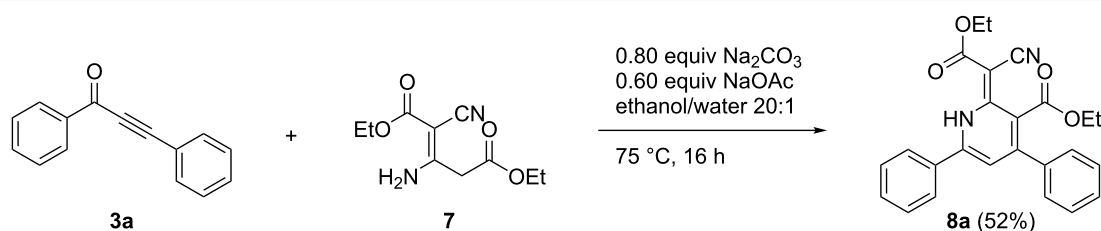


Scheme 7: Formation of 1*H*-pyridine **5b** starting from alkynone **3d** having an electron-withdrawing substituent.

dimer **7** in hand, we performed the reaction at 75 °C for 16 h, but we only could isolate 1*H*-pyridine **8a**, which still contains an ester group (Scheme 8). Therefore, the in situ formation of the dimer starting from the alkynone **3a** and ethyl cyanoacetate (**4**) was excluded for the formation of the 1*H*-pyridine **5a**.

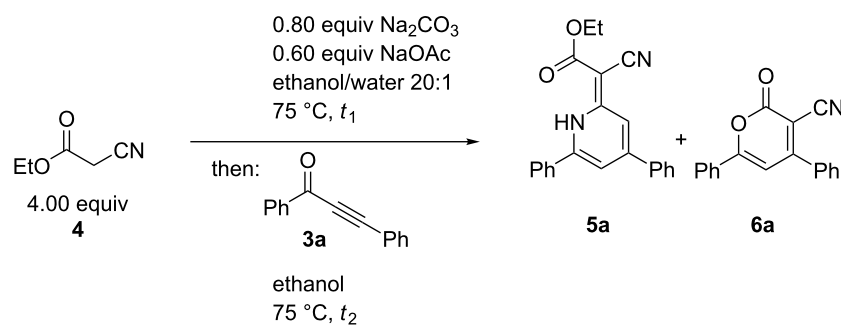
While the in situ generation of dimer **7** does not happen during the formation of 1*H*-pyridine **5a**, we examined the reaction between ethyl cyanoacetate (**4**) and the optimized base system by adding alkynone **3a** to the reaction after different times (Table 3).

In the first attempt, alkynone **3a** was added after 2 h. 1*H*-Pyridine **5a** was isolated in 53% yield (Table 3, entry 1), indicating that the time of addition of the alkynone is not relevant within the first two hours of the reaction. However, if alkynone **3a** was added after 6 h α -pyrone **6a** was the main product and 1*H*-pyridine **5a** could only be isolated in 5% yield (Table 3, entry 2). Upon the addition of alkynone **3a** after 24 h, both 1*H*-pyridine **5a** and α -pyrone **6a** were isolated in only around 3% yield. This finding supports that within the first two hours ethyl cyanoacetate (**4**) is consumed and thereafter the ethyl cyanoacetate concentration is just too low for the formation of 1*H*-pyridine



Scheme 8: Formation of 1*H*-pyridine **8a** by Michael addition–cyclocondensation reaction.

Table 3: Influence of the reaction time on the self-condensation of ethyl cyanoacetate (**4**) in the presence of the optimized base system.^a



Entry	t_1	t_2	Compound 5a (yield) ^b	Compound 6a (yield) ^b
1	2 h	16 h	53%	–
2	6 h	16 h	5%	46%
3	24 h	16 h	3%	2%

^aAll reactions were carried out on a 0.500 mmol scale ($c_0(\mathbf{3a}) = 0.50 \text{ M}$, $c_0(\mathbf{4}) = 2.0 \text{ M}$); ^ball yields refer to isolated and purified products.

5a, therefore α -pyrone **6a** is formed. At longer initial reaction times (6 and 24 h) there is no ethyl cyanoacetate (**4**) left for the formation of any product. Also, ethyl cyanoacetate (**4**) probably does not form dimer **7** because in that case under these conditions *1H*-pyridine **8a** would have been detected.

Therefore, the tentative mechanistic rationale takes into account that the formation of *1H*-pyridine **5a** rather proceeds via stepwise condensation of alkyne **3** with two equivalents of ethyl cyanoacetate (**4**) than by reaction with dimer **7** (Scheme 9).

First, a molecule of ethyl cyanoacetate (**4**) attacks the alkyne **3a** in a Michael addition. A second molecule **4** then attacks the cyano substituent and an imine is formed. The ester substituent of the initially reacted more electrophilic ethyl cyanoacetate (**4**) is presumably cleaved by a base-mediated acyl cleavage furnishing directly *1H*-pyridine **5a** after protonation.

For examining the influence of the electronic nature of the alkyne **3** on the product formation, a range of differently substituted alkynes **3** (for experimental details on their preparation, see chapters 2.1 and 2.2 in Supporting Information File 1) bearing electron-donating and/or electron-withdrawing substituents were synthesized and employed in the cyclocondensation step under the optimized reaction conditions [32-34]. Alkynes **3b–e** with only one electron-donating substituent furnish the corresponding α -pyrones **6b–e**, while the alkyne with a single electron-withdrawing substituent furnishes *1H*-pyridines **5b–e**. Interestingly, the position of substitution on the alkyne does not affect the outcome (Table 4, entries 2 and 6). Also, for alkyne **3j** bearing an electron-donating substituent on either aryl ring, α -pyrone **6f** is formed likewise (Table 4,

entry 10). For electronically unsymmetrically substituted alkynes **3** the product formation depends rather on the strength of the employed electron-donating group. Whereas the *p*-anisyl substituent leads to the formation of *1H*-pyridine (Table 4, entries 11 and 12), the *N,N*-dimethylaminophenyl substituent furnishes α -pyrone **6g** (Table 4, entry 13).

For synthesizing *1H*-pyridine derivatives **8** with an electron-donating group we employed the isolated dimer **7** and were able to isolate *1H*-pyridines **8** in 52 and 34% yield (Scheme 10).

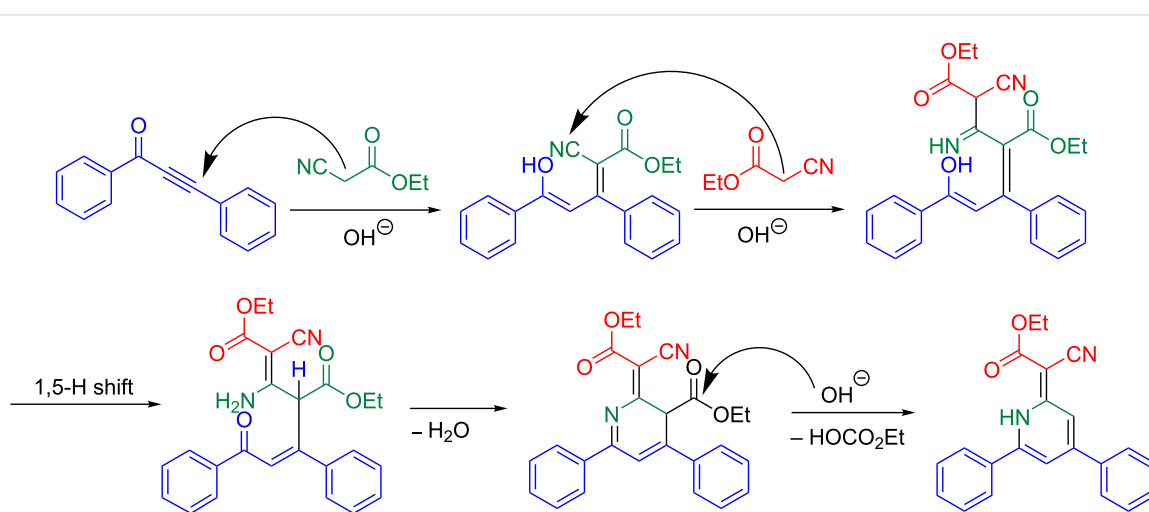
Crystal structure of *1H*-pyridine **5a**

The structure of *1H*-pyridines **5** was further corroborated by a single crystal X-ray structure determination of compound **5a** (Figure 1) [35]. In the single crystal the carboxyl ester group is oriented to the N–H and via a hydrogen bond. Solid-state torsional/dihedral angles between the 4- and 6-positioned aryl rings differ especially for the 6-positioned phenyl ring with 27° in the X-ray structure and 38° from calculation (for comparison to the DFT calculated ground state structure of *1H*-pyridine **5a**, see chapter 12.3 in Supporting Information File 1). This is probably due to packing constraints from the involvement of the 6-phenyl ring in C–H...N [36-39] and C–H... π [40-49] interactions (Figure 2, for details, see Supporting Information File 1). It is noteworthy to mention that there are no significant π ... π interactions in the solid-state structure of **5a** (for details, see Supporting Information File 1) [50-57].

Photophysical properties

Photophysical properties of *1H*-pyridines **5** and **8**

1H-Pyridine derivatives **5** are yellow or orange compounds under daylight (Figure 3, top) and fluoresce in solution (Figure 3, center) and in the solid state (Figure 3, bottom).

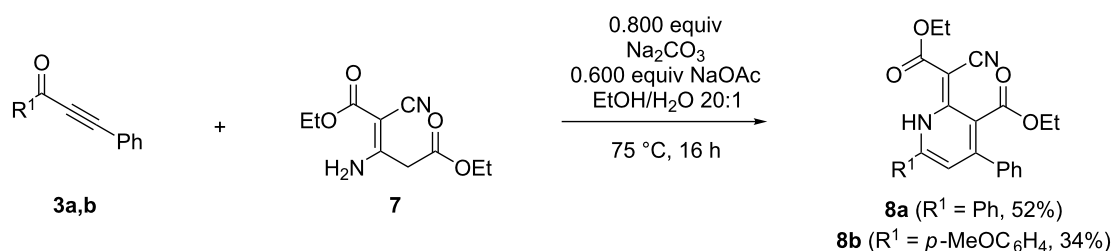


Scheme 9: Mechanistic rationale for the formation of the *1H*-pyridine **5a**.

Table 4: Michael addition–cyclocondensation synthesis of 1*H*-pyridine **5** or α -pyrone **6**.

Entry	Alkynone 3	1 <i>H</i> -Pyridine 5 ^a	α -Pyrone 6 ^a
1	3a (R ¹ = Ph, R ² = Ph)	5a (R ¹ = Ph, R ² = Ph, 56%)	–
2	3b (R ¹ = <i>p</i> -MeOC ₆ H ₄ , R ² = Ph)	–	6b (R ¹ = <i>p</i> -MeOC ₆ H ₄ , R ² = Ph; 70%)
3	3c (R ¹ = <i>p</i> -Me ₂ NC ₆ H ₄ , R ² = Ph)	–	6c (R ¹ = <i>p</i> -Me ₂ NC ₆ H ₄ , R ² = Ph, 12%)
4	3d (R ¹ = <i>p</i> -F ₃ CC ₆ H ₄ , R ² = Ph)	5b (R ¹ = <i>p</i> -F ₃ CC ₆ H ₄ , R ² = Ph, 22%)	–
5	3e (R ¹ = <i>p</i> -NCC ₆ H ₄ , R ² = Ph)	5c (R ¹ = <i>p</i> -NCC ₆ H ₄ , R ² = Ph, 20%)	–
6	3f (R ¹ = Ph, R ² = <i>p</i> -MeOC ₆ H ₄)	–	6d (R ¹ = Ph, R ² = <i>p</i> -MeOC ₆ H ₄ , 82%)
7	3g (R ¹ = Ph, R ² = <i>p</i> -Me ₂ NC ₆ H ₄)	–	6e (R ¹ = Ph, R ² = <i>p</i> -Me ₂ NC ₆ H ₄ , 62%)
8	3h (R ¹ = Ph, R ² = <i>p</i> -F ₃ CC ₆ H ₄)	5d (R ¹ = Ph, R ² = <i>p</i> -F ₃ CC ₆ H ₄ , 25%)	–
9	3i (R ¹ = Ph, R ² = <i>p</i> -NCC ₆ H ₄)	5e (R ¹ = Ph, R ² = <i>p</i> -NCC ₆ H ₄ , 2%)	–
10	3j (R ¹ = <i>p</i> -MeOC ₆ H ₄ , R ² = <i>p</i> -MeOC ₆ H ₄)	–	6f (R ¹ = <i>p</i> -MeOC ₆ H ₄ , R ² = <i>p</i> -MeOC ₆ H ₄ , 45%)
11	3k (R ¹ = <i>p</i> -MeOC ₆ H ₄ , R ² = <i>p</i> -F ₃ CC ₆ H ₄)	5f (R ¹ = <i>p</i> -MeOC ₆ H ₄ , R ² = <i>p</i> -F ₃ CC ₆ H ₄ , 37%)	–
12	3l (R ¹ = <i>p</i> -F ₃ CC ₆ H ₄ , R ² = <i>p</i> -MeOC ₆ H ₄)	5g (R ¹ = <i>p</i> -F ₃ CC ₆ H ₄ , R ² = <i>p</i> -MeOC ₆ H ₄ , 40%)	–
13	3m (R ¹ = <i>p</i> -F ₃ CC ₆ H ₄ , R ² = <i>p</i> -Me ₂ NC ₆ H ₄)	–	6g (R ¹ = <i>p</i> -F ₃ CC ₆ H ₄ , R ² = <i>p</i> -Me ₂ NC ₆ H ₄ , 71%)
14	3n (R ¹ = 2-thienyl, R ² = Ph)	5h (R ¹ = 2-thienyl, R ² = Ph, 51%)	–

^aAll yields refer to isolated and purified products.

**Scheme 10:** Formation of 1*H*-pyridine **8a** from alkynone **3b** and dimer **7**.

Therefore, the photophysical properties were studied by absorption and emission spectroscopy (Figure 4, Table 5).

All compounds show three absorption maxima at around 275, 320 and 430 nm, where the longest wavelength absorption maxima exhibit extinction coefficients of around 9500 L·mol⁻¹·cm⁻¹ (Table 5). Upon introducing electron-withdrawing substituents on the aryl rings the longest wavelength maxima shift bathochromically (Table 5, entries 2–5). The redshift qualitatively corresponds with the strength of the acceptor group (Table 5, entries 3 and 5). However, as can be seen from entries 2–5 (Table 5), the placement of the acceptor

group at the 4 or 6-aryl substituent does not affect the absorption energies. This situation changes to a minor extent upon placing an additional donor substituent at the remaining phenyl substituent (Table 5, entries 6 and 7). A thienyl substituent instead of a phenyl substituent causes a redshift of the longest wavelength absorption maximum (Table 5, entries 1 and 8).

Upon excitation at the longest wavelength absorption band dichloromethane solutions of all compounds **5** fluoresce with emission maxima at around 565 nm (Table 5, entries 2–5). Upon the introduction of electron-withdrawing substituents the maxima are shifted bathochromically, similarly as the absorp-

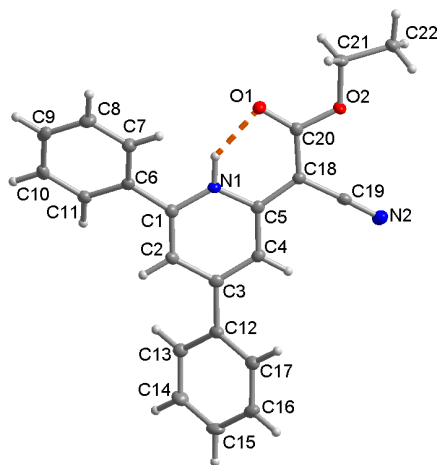


Figure 1: Molecular structure of *1H*-pyridine **5a** (50% thermal ellipsoids), showing the intramolecular N–H···O bond as dashed orange line. H-bond details N1–H 0.90(2) Å, H···O1 1.87(2) Å, N1···O2 2.624(2) Å, O1–H···O2 140(1)°.

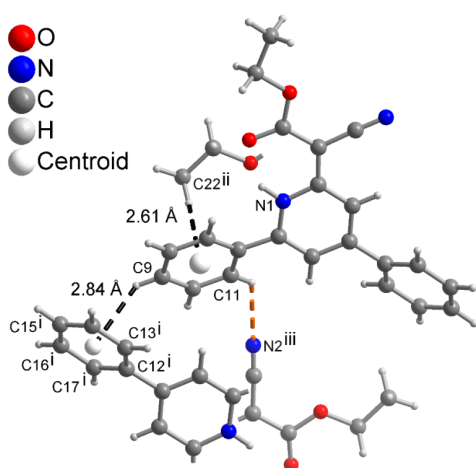


Figure 2: Supramolecular C–H···N [36–39] and C–H··· π [40–49] interactions around the 6-positioned phenyl ring in **5a**. Details of C–H···N bond (dashed orange line) C11–H 0.95 Å, H···N2 2.61 Å, C11···N2 3.263(2) Å, C11–H···N2 127°. Symmetry transformations are $i = 1-x, 1-y, 1-z$; $ii = x, 3/2-y, -1/2+z$, $iii = 1-x, -1/2+y, -1/2-z$.

tion maxima, and the shift is qualitatively correlated with the acceptor strength. In comparison, the introduction of another electron-donating substituent does not significantly change the luminescence characteristics (Table 5, entries 2, 4, 6 and 7). The Stokes shifts fall in a range between 5000 and 6100 cm^{-1} and the fluorescence quantum yields of the *1H*-pyridines **5** account between 1 and 3%.

Besides solution fluorescence all *1H*-pyridines **5** also luminesce in the solid state (Figure 3, bottom). The emission maxima of two selected *1H*-pyridines **5** were determined

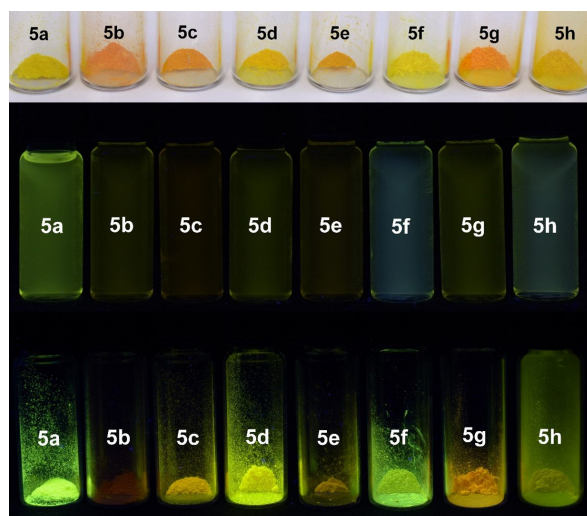


Figure 3: *1H*-Pyridine derivatives **5** as solids under daylight (top), under UV light ($\lambda_{\text{exc}} = 365 \text{ nm}$, $c(\mathbf{5}) = 10^{-4} \text{ M}$) in dichloromethane solution (center), and under UV light ($\lambda_{\text{exc}} = 365 \text{ nm}$) in the solid state (bottom).

(Figure 5, Table 6), showing a similar behavior in the solid state as in solution. The emission maximum of the unsubstituted *1H*-pyridine **5a** appears at 540 nm, while the CF_3 -substituted *1H*-pyridine **5b** emits bathochromically shifted at 604 nm.

In addition, both ester-substituted *1H*-pyridines **8a** and **8b** also possess interesting photophysical properties (Figure 6, Table 7). Under daylight they are yellow and they fluoresce in solution and in the solid state. The three absorption maxima are found at around 270, 315 and 415 nm. The methoxy group in the spectrum of compound **8b** only has a minor influence on the absorption maximum, however, slightly more on the emission maximum. The fluorescence quantum yields Φ_f of both compounds are lower than 1%.

With the addition of the second ester group in the 3-position to *1H*-pyridine **8a** the fluorescence in the solid state appears to shift to blue. If the phenyl substituent in the 4-position bears an additional methoxy substituent the fluorescence of the *1H*-pyridine **8b** appears yellow again (Figure 7).

Photophysical properties of α -pyrones **6**

All α -pyrone derivatives **6** are yellow or red under daylight (Figure 8, top) and some of them fluoresce in solution (Figure 8, center) and in the solid state (Figure 8, bottom). Therefore, the photophysical properties were studied by absorption and emission spectroscopy (Figure 9, Table 8).

All compounds show 2–4 absorption maxima and the shortest wavelength maxima appear at around 255 nm. The unsubsti-

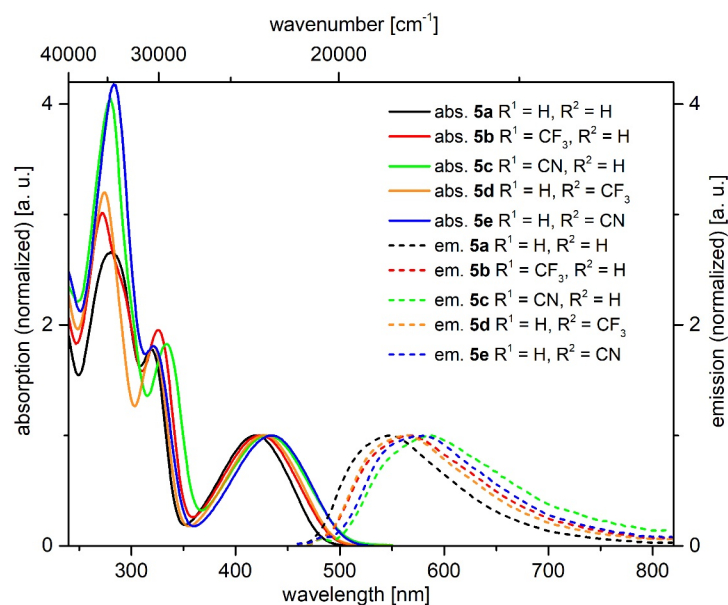


Figure 4: Selected normalized absorption (solid lines) and emission (dashed lines) spectra of 1*H*-pyridines **5a–e** (recorded in dichloromethane at $T = 298$ K).

Table 5: Photophysical properties of 1*H*-pyridines **5**.

Entry	Compound	R ¹	R ²	$\lambda_{\max, \text{abs}}$ [nm] ^a (ϵ [L·mol ⁻¹ ·cm ⁻¹])	$\lambda_{\max, \text{em}}$ [nm] ^b (Φ_f) ^c	Stokes shift $\Delta\tilde{\nu}$ [cm ⁻¹]
1	5a	Ph	Ph	281 (26100), 319 (17400), 418 (9800)	545 (0.02)	5600
2	5b	<i>p</i> -F ₃ CC ₆ H ₄	Ph	272 (27000), 326 (17500), 424 (8900)	565 (0.01)	5600
3	5c	<i>p</i> -NCC ₆ H ₄	Ph	280 (37600), 333 (17300), 431 (9500)	585 (0.01)	6100
4	5d	Ph	<i>p</i> -F ₃ CC ₆ H ₄	274 (32000), 321 (18100), 428 (10000)	565 (0.01)	5700
5	5e	Ph	<i>p</i> -NCC ₆ H ₄	283 (36000), 322 (15600), 434 (8600)	579 (0.01)	5800
6	5f	<i>p</i> -MeOC ₆ H ₄	<i>p</i> -F ₃ CC ₆ H ₄	261 (26200), 306 (28400), 429 (10400)	557 (0.02)	5400
7	5g	<i>p</i> -F ₃ CC ₆ H ₄	<i>p</i> -MeOC ₆ H ₄	260 (20300), 324 (43800), 420 (10000)	562 (0.02)	6000
8	5h	2-thienyl	Ph	273 (21800), 308 (26700), 433 (9200)	560 (0.03)	5200

^aRecorded in dichloromethane, $T = 293$ K, $c(\mathbf{5}) = 10^{-6}$ M; ^brecorded in dichloromethane, $T = 293$ K, $c(\mathbf{5}) = 10^{-7}$ M; ^cfluorescence quantum yields were determined relative to coumarin153 ($\Phi_f = 0.54$) as a standard in ethanol [58].

tuted α -pyrone **6a** exhibits its longest wavelength maximum at 381 nm (Table 8, entry 1). A *p*-methoxyphenyl substituent in the 6-position causes a bathochromic shift (Table 8, entry 2), whereas the same substituent in 4-position leads to a hypsochromic shift (Table 8, entry 4). Interestingly, *p*-methoxyphenyl substituents at positions 4 and 6 split the longest absorption band into two maxima at 358 nm (arising from the *p*-methoxyphenyl substituent in the 4-position and at 400 nm arising from the *p*-methoxyphenyl substituent in the 6-position) (Table 8, entry 6). The introduction of a more strongly electron-donating substituent, such as *N,N*-dimethylaminophenyl, causes a significant bathochromic shift (Table 8, entries 3 and 5). Donor–acceptor substitution in positions 4 and 6 causes a further bathochromic shift (Table 8, entry 7).

In solution only *N,N*-dimethylaminophenyl-substituted derivatives fluoresce (Figure 10). While the 6-substituted α -pyrone **6c** has a fluorescence maximum at 567 nm, the one for the regioisomer **6e** is shifted bathochromically to 634 nm (Table 8, entries 3 and 5). Donor–acceptor substitution in positions 4 and 6 causes a further bathochromic shift to 673 nm (Table 8, entry 7). Most remarkably, the regioisomers **6c** and **6e** differ quite significantly with respect to their fluorescence quantum yields Φ_f . While chromophore **6e** only emits with an efficiency of 1%, the regioisomer **6c** accounts for an extraordinarily high relative quantum yield of 99%.

Furthermore, the *N,N*-dimethylaminophenyl-derivative **6c** shows a pronounced emission solvatochromism (Figure 11,

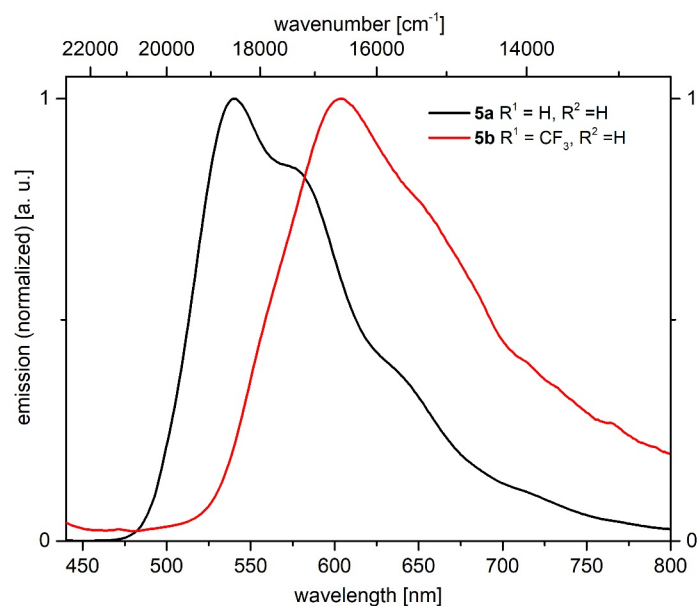


Figure 5: Selected normalized emission spectra of 1*H*-pyridine **5a** and **5b** in the solid state at $T = 298$ K.

Table 6: Photophysical properties of 1*H*-pyridines **5a** and **5b** in the solid state.

Compound	R ¹	R ²	$\lambda_{\text{max,em}}$ [nm] ^a
5a	H	H	540
5b	CF ₃	H	604

^a $\lambda_{\text{exc}} = 420$ nm.

Table 9). While the polarity effect on the absorption maximum is only minor within a range of the longest wavelength maximum between 469 and 490 nm, the emission maximum is shifted bathochromically with increasing solvent polarity in a range from green fluorescence (529 nm) in toluene to red fluorescence in DMSO (638 nm) (Figure 12). The observed positive emission solvatochromism is a consequence of a significant change in the dipole moment from the electronic ground to

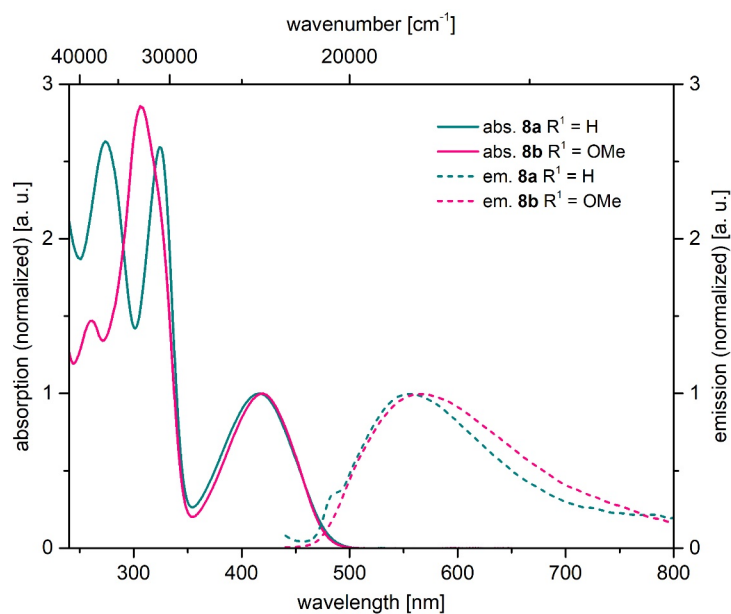
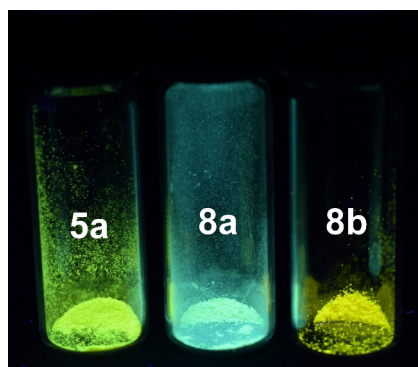


Figure 6: Selected normalized absorption (solid lines) and emission (dashed lines) spectra of 1*H*-pyridines **8a** and **8b** (recorded in dichloromethane at $T = 298$ K).

Table 7: Photophysical properties of 1*H*-pyridines **8**.

Compound	R ¹	R ²	$\lambda_{\max, \text{abs}}$ [nm] ^a (ϵ [L·mol ⁻¹ ·cm ⁻¹])	$\lambda_{\max, \text{em}}$ [nm] ^b (Φ_f) ^c	Stokes shift $\Delta \tilde{\nu}$ [cm ⁻¹]
8a	Ph	Ph	274 (20300), 324 (20100), 417 (7700)	557 (<0.01)	6000
8b	<i>p</i> -MeOC ₆ H ₄	Ph	261 (16200), 307 (31300), 419 (11000)	565 (<0.01)	6200

^aRecorded in dichloromethane, $T = 293$ K, $c(\mathbf{8}) = 10^{-6}$ M; ^brecorded in dichloromethane, $T = 293$ K, $c(\mathbf{8}) = 10^{-7}$ M ($\lambda_{\text{exc}} = 420$ nm); ^cfluorescence quantum yields were determined relative to coumarin153 ($\Phi_f = 0.54$) as a standard in ethanol [58].

**Figure 7:** Solid-state luminescence of 1*H*-pyridines **5a**, **8a** and **8b** ($\lambda_{\text{exc}} = 365$ nm).

the vibrationally relaxed excited state [59]. Plotting Stokes shifts $\Delta \tilde{\nu}$ against the orientation polarizabilities Δf of the respective solvents (Lippert plot) [60] gives a reasonable linear correlation with a moderate fit of $r^2 = 0.970$ (Figure 13). The orientation polarizabilities Δf were calculated according to Equation 1

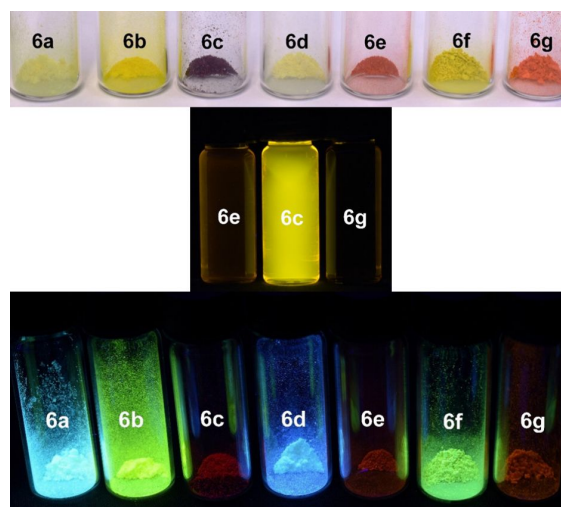
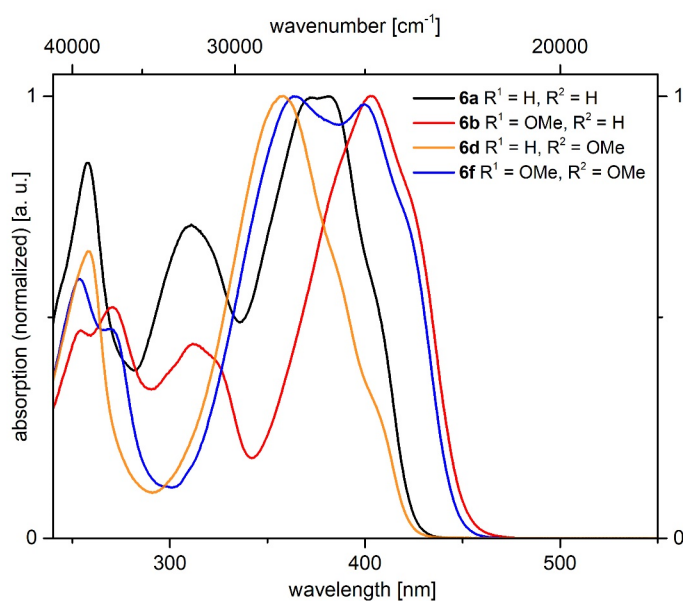
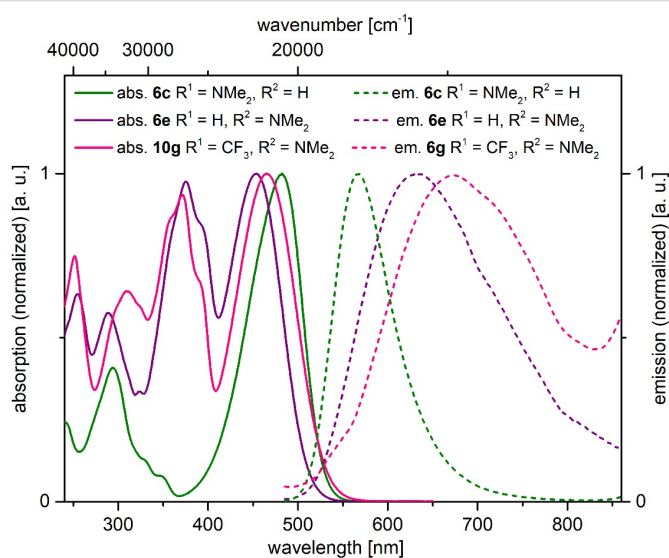
**Figure 8:** α -Pyrone **6** as solids under daylight (top), selected derivatives under UV light ($\lambda_{\text{exc}} = 365$ nm, $c(\mathbf{6}) = 10^{-4}$ M) in dichloromethane solution (center), and under UV light ($\lambda_{\text{exc}} = 365$ nm) in the solid state (bottom).**Figure 9:** Selected normalized absorption spectra of α -pyrone **6a**, **6b**, **6d**, and **6e** recorded in dichloromethane at $T = 298$ K.

Table 8: Photophysical properties of α -pyrones **6**.

Entry	Compound	R ¹	R ²	$\lambda_{\max,abs}$ [nm] ^a (ϵ [L·mol ⁻¹ ·cm ⁻¹])	$\lambda_{\max,em}$ [nm] ^b (Φ_f) ^c	Stokes shift $\Delta\tilde{\nu}$ [cm ⁻¹]
1	6a	Ph	Ph	258 (15300), 311 (12800), 381 (18000)	–	–
2	6b	<i>p</i> -MeOC ₆ H ₄	Ph	254 (10300), 271 (11500), 312 (9600), 404 (21900)	–	–
3	6c	<i>p</i> -Me ₂ NC ₆ H ₄	Ph	294 (18800), 482 (47300)	567 (0.99)	3100
4	6d	Ph	<i>p</i> -MeOC ₆ H ₄	258 (19700), 358 (30400)	–	–
5	6e	Ph	<i>p</i> -Me ₂ NC ₆ H ₄	255 (25600), 289 (23300), 375 (39600), 453 (40600)	634 (0.01)	6300
6	6f	<i>p</i> -MeOC ₆ H ₄	<i>p</i> -MeOC ₆ H ₄	254 (15000), 364 (25600), 400 (25100)	–	–
7	6g	<i>p</i> -F ₃ CC ₆ H ₄	<i>p</i> -Me ₂ NC ₆ H ₄	251 (16200), 309 (13900), 372 (20200), 465 (21600)	673 (<0.01)	6600

^aRecorded in dichloromethane, $T = 293$ K, $c(\mathbf{6}) = 10^{-6}$ M; ^brecorded in dichloromethane, $T = 293$ K, $c(\mathbf{6}) = 10^{-7}$ M ($\lambda_{exc} = 465$ nm); ^cfluorescence quantum yields were determined relative to DCM ($\Phi_f = 0.435$) as a standard in ethanol [58].

**Figure 10:** Selected normalized absorption (solid lines) and emission (dashed lines) spectra of α -pyrones **6c**, **6e**, and **6g** recorded in dichloromethane at $T = 298$ K.**Figure 11:** Absorption (top) and fluorescence (bottom) of compound **6c** with variable solvent polarity (left to the right: toluene, ethyl acetate, acetone, DMF and DMSO, $c(\mathbf{6c}) = 10^{-4}$ M; $\lambda_{exc} = 365$ nm, handheld UV lamp).

$$\Delta f = \frac{\epsilon_r - 1}{2 \cdot \epsilon_r + 1} - \frac{n^2 - 1}{2 \cdot n^2 + 1} \quad (1)$$

where ϵ_r is the relative permittivity and n the optical refractive index of the respective solvent.

The change in dipole from the ground to the excited state can be calculated according to the Lippert–Mataga equation (Equation 2)

$$\tilde{\nu}_{abs} - \tilde{\nu}_{em} = \frac{2\Delta f}{4 \cdot \pi \cdot \epsilon_0 \cdot h \cdot c \cdot a^3} \cdot (\mu_E - \mu_G)^2 + const \quad (2)$$

where $\tilde{\nu}_{abs}$ represents the absorption and $\tilde{\nu}_{em}$ the emission maxima (in m^{-1}), μ_E and μ_G are the dipole moments in the

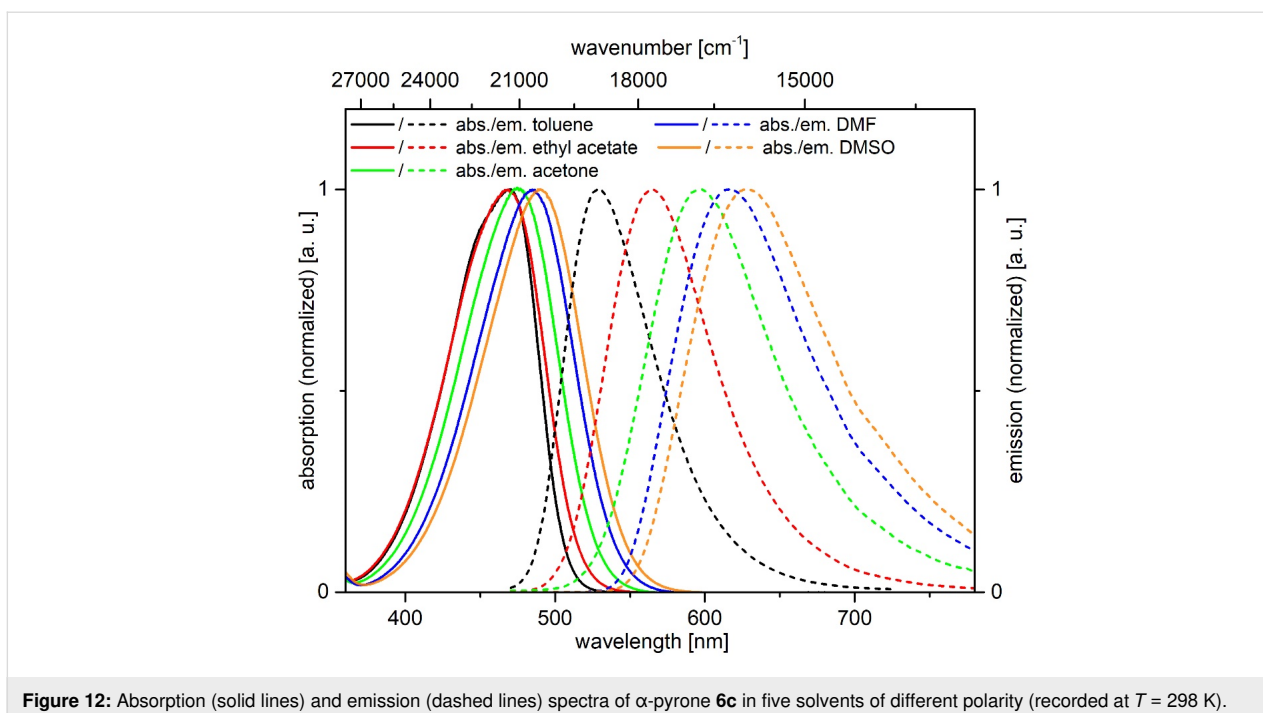


Figure 12: Absorption (solid lines) and emission (dashed lines) spectra of α -pyrone **6c** in five solvents of different polarity (recorded at $T = 298$ K).

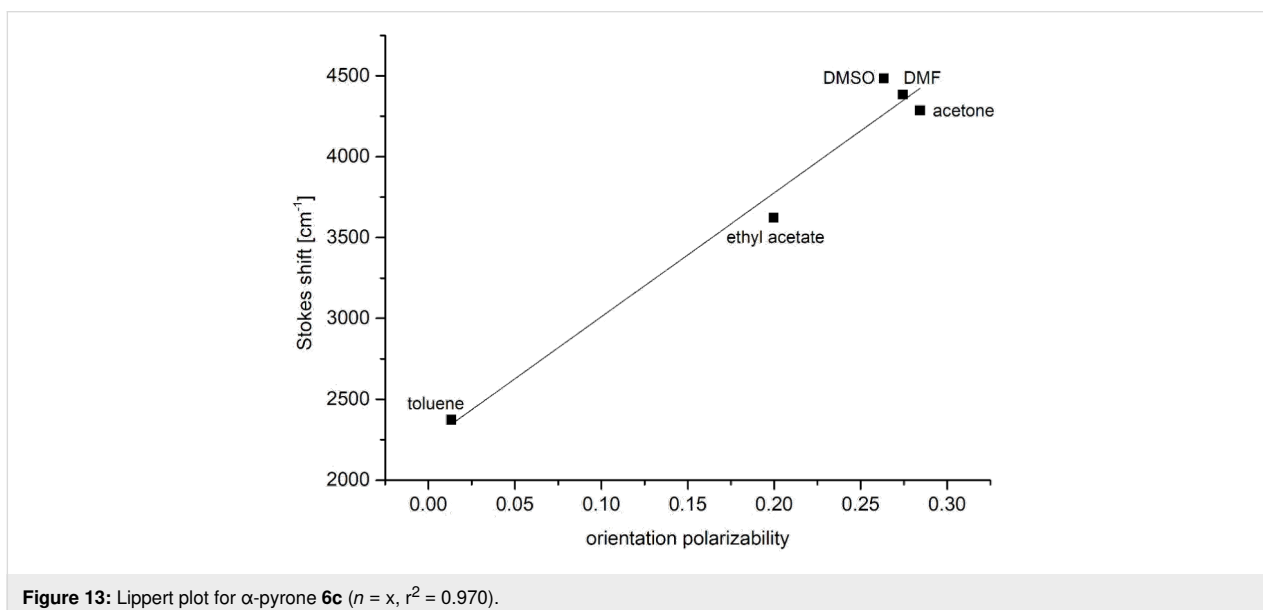


Figure 13: Lippert plot for α -pyrone **6c** ($n = x$, $r^2 = 0.970$).

excited and ground state (in C·m), ϵ_0 ($8.8542 \cdot 10^{-12}$ A·s/V·m) is the vacuum permittivity constant, h ($6.6256 \cdot 10^{-34}$ J·s) is the Planck's constant, c ($2.9979 \cdot 10^{10}$ cm/s) is the speed of light and a is the radius of the solvent cavity occupied by the molecules (in m). The Onsager radius a , assuming a spherical dipole to approximate the molecular volume of the molecule in solution, was estimated from the optimized ground-state structure of compound **6c** obtained by DFT calculations. With an a value of 5.46 Å, the change in dipole moment was calculated to 11.6 D ($3.87 \cdot 10^{-29}$ C·m).

All α -pyrones **6** fluoresce in the solid state (Figure 8, bottom) and for five selected α -pyrones **6** the emission maxima were determined (Figure 14, Table 9). The fluorescence maximum of unsubstituted α -pyrone **6a** lies at 499 nm and the maxima of the monomethoxy-substituted regioisomers **6b** (540 nm) and **6d** (489 nm) appear at quite different energies, similar to their corresponding absorption maxima in solution. In comparison to α -pyrone **6a** the introduction of two methoxy substituents in derivative **6f** results in a bathochromic shift to 526 nm. The solid-state emission of N,N -dimethylaminophenyl derivative **6c**

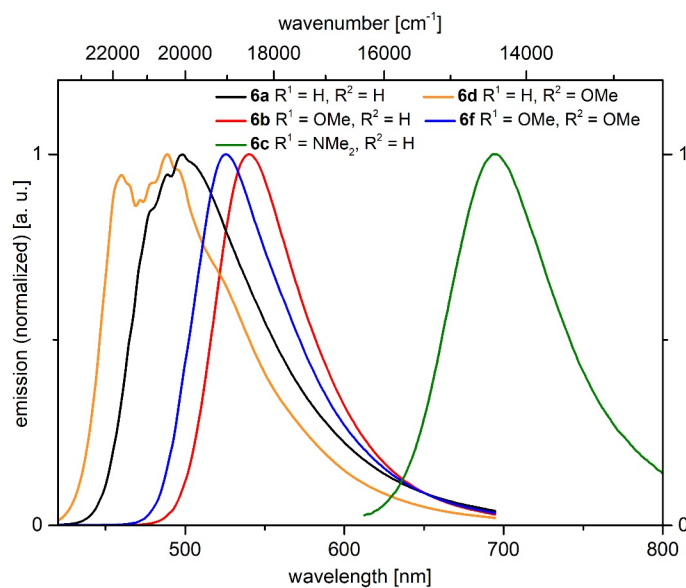


Figure 14: Normalized emission spectra of selected α -pyrones **6a–d,f** in the solid state at $T = 298$ K.

Table 9: Photophysical properties of selected α -pyrones **6** in the solid state.

Compound	R ¹	R ²	$\lambda_{\text{max,em}}$ [nm] ^a
6a	Ph	Ph	499
6b	<i>p</i> -MeOC ₆ H ₄	Ph	540
6c	<i>p</i> -Me ₂ NC ₆ H ₄	Ph	694 ^b
6d	Ph	<i>p</i> -MeOC ₆ H ₄	489
6f	<i>p</i> -MeOC ₆ H ₄	<i>p</i> -MeOC ₆ H ₄	526

^a $\lambda_{\text{exc}} = 380$ nm; ^b $\lambda_{\text{exc}} = 480$ nm.

shows an enormous redshift to 694 nm. The solid-state fluorescence quantum yield Φ_f of compound **6c** was determined to 11%.

Interestingly, the α -pyrone **6e** with the *N,N*-dimethylamino-phenyl substituent in 4-position only fluoresces weakly in solution but shows a strong fluorescence in the solid state. This finding suggests that by restricting intramolecular motion and vibration, which enables radiation-less deactivation of the excited state [61], an AIE (aggregation-induced emission) or AIEE (aggregation-induced enhanced emission), might become operative [62–64].

The AIE or AIEE effect was assessed by measuring the emission spectra of α -pyrone **6e** in THF/water at variable ratios (Figure 15). In pure THF α -pyrone **6e** displays an emission maximum at 644 nm with a relative intensity of 54. The addition of water first quenches the fluorescence and at a water/THF

ratio of 80% aggregates are formed and the emission maximum is shifted to 632 nm. The maximal relative intensity of 130 is reached for a ratio of 85%, which is more intense than in pure THF, therefore, an AIEE effect occurs. Further increasing the water content slightly quenches the emission.

Computational studies

Computational studies on 1*H*-pyridines **5** and **8**

For a further elucidation of the electronic structure the geometries of the electronic ground-state structures of the 1*H*-pyridines **5** and **8** were optimized using Gaussian 09 with the B3LYP functional [65–68] and the Pople 6-311G** basis set [69], applying vacuum calculations as well as the polarizable continuum model (PCM) with dichloromethane as a solvent [70] (for details of the DFT calculations, see Supporting Information File 1). The optimized geometries were verified by frequency analyses of the local minima. The electronic absorptions of the 1*H*-pyridines **5** and **8** were calculated on the level of TDDFT theory employing the B3LYP functional and the Pople 6-311G** basis set. The calculated absorption maxima are in accordance with the experimentally determined maxima (for details, see Tables S7 and S8 in Supporting Information File 1). Most characteristically, for all 1*H*-pyridines **5** and **8** the longest wavelength maxima representing the Franck–Condon S₁ states are characterized by HOMO–LUMO transitions and S₂ states are represented by HOMO–LUMO+1 transitions.

The computed Kohn–Sham frontier molecular orbitals show that the coefficient density of the HOMO of the 1*H*-pyridines **5f** and **5g** with an electron-withdrawing and an electron-donating

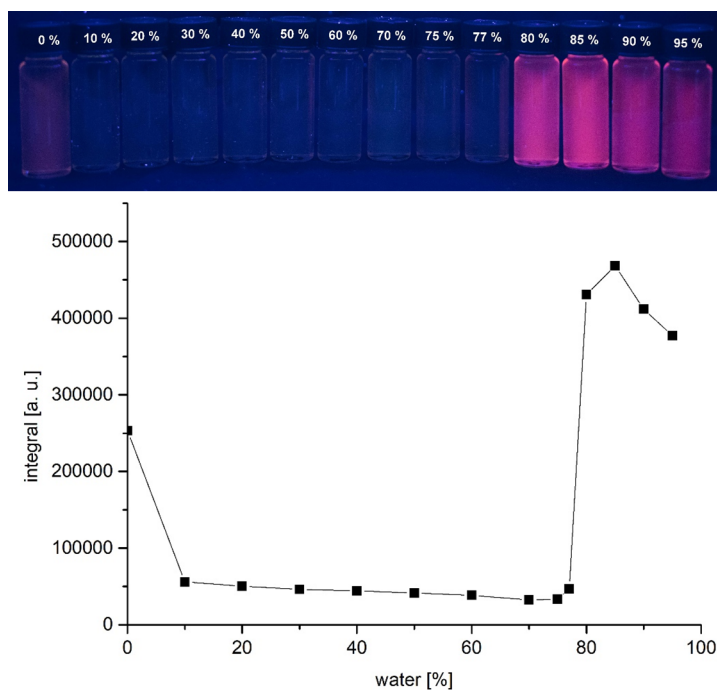


Figure 15: Fluorescence of compound **6e** in different THF/water fractions (top, $\lambda_{\text{exc}} = 365$ nm, handheld UV lamp) and I/I_0 vs %H₂O of α -pyrone **6e** in THF/water mixtures containing different water fractions (bottom, recorded at $T = 298$ K).

substituent is located on the *1H*-pyridine core, the ester and cyano substituents and also on the electron-rich aryl substituent. For the LUMO, the coefficient density is spread over the whole scaffold (Figure 16).

Computational studies on α -pyrones **6**

For further elucidation of the electronic structure the geometries of the electronic ground-state structures of the α -pyrones

6 were optimized using Gaussian 09 with the B3LYP functional [65–68] and the Pople 6-311G** basis set [69], applying vacuum calculations as well as the polarizable continuum model (PCM) with dichloromethane as a solvent [70] (for details on the DFT calculations, see Supporting Information File 1). The optimized geometries were verified by frequency analyses of the local minima. The electronic absorptions of the α -pyrones **6** were calculated on the level of TDDFT theory em-

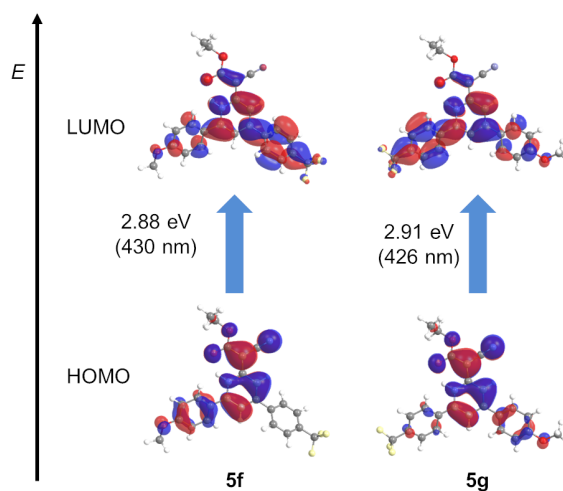


Figure 16: Selected DFT-computed (B3LYP 6-311G**) Kohn–Sham FMOs for *1H*-pyridines **5f** and **5g** representing contributions of the longest wavelength Franck–Condon absorption bands.

ploying the B3LYP functional and the Pople 6-311G** basis set. The calculated absorption maxima are in accordance with the experimentally determined maxima (for details, see Table S10 in Supporting Information File 1). For all α -pyrones **6** the longest wavelength maxima are characterized by Franck–Condon S_1 states representing HOMO–LUMO transitions (Figure 17).

The computed Kohn–Sham frontier molecular orbitals show that the coefficient density of the HOMO in the parent α -pyrone **6a** is localized on the α -pyrone core and on the phenyl substituent in the 6-position. For an *N,N*-dimethylaminophenyl substituent, there is no difference, but for an *N,N*-dimethylamino-phenyl substituent in the 4-position the coefficient density is shifted towards this substituent. With electron-donating substituents in the 4- and 6-position, the coefficient density is again located on the core and the phenyl substituent in 6-position. Donor substituents in 4-position and acceptor substituents in 6-position cause a coefficient density shift towards the 4-substituent. The coefficient density in the LUMO in all compounds is spread over the whole scaffold.

Conclusion

The cyclocondensation of alkynones and ethyl cyanoacetate, depending on the reaction conditions, the type of base, and the reaction temperature, as well as the electronic nature of the alkynone **3** furnishes either *1H*-pyridines or α -pyrones. Optimized reaction conditions finally give rise to 8 examples of *1H*-pyridines and 6 examples of α -pyrones. While the presence of electron-withdrawing substituents mainly furnish *1H*-pyridines and electron-donating groups lead to the forma-

tion of α -pyrones. The strongly electron-donating *p*-*N,N*-dimethylaminophenyl group furnishes α -pyrones.

1H-Pyridines absorb and emit intensively in solution and in the solid state. While the absorption behavior is not affected by the substitution pattern the emission maxima are shifted bathochromically with increasing acceptor strength. The same trend manifests for the solid-state emission.

For α -pyrones the photophysical properties are considerably depending on the substituent pattern. The absorption and emission maxima are shifted bathochromically with increasing donor strength. α -Pyrones are only weakly fluorescent in solution. However, with distinct *p*-*N,N*-dimethylaminophenyl substitution in 6-position, an extraordinarily high fluorescence quantum yield of 99% in solution and 11% in the solid state was achieved. Interestingly, the isomeric *p*-*N,N*-dimethylamino-phenyl substitution in 6-position represents a system with aggregation-induced emission enhancement. These design principles of luminescent *1H*-pyridines and α -pyrones as polarity sensitive tunable luminophores and the observed aggregation-induced emission enhancement are currently under further investigation.

Experimental

Typical procedure for the cyclocondensation synthesis of compound **5d**

1-Phenyl-3-[4-(trifluoromethyl)phenyl]prop-2-yn-1-one (**3h**, 1.40 g, 5.00 mmol), was placed in a dry Schlenk tube and ethanol (10 mL) was added. Sodium carbonate (430 mg, 4.00 mmol), sodium acetate (250 mg, 3.00 mmol), water

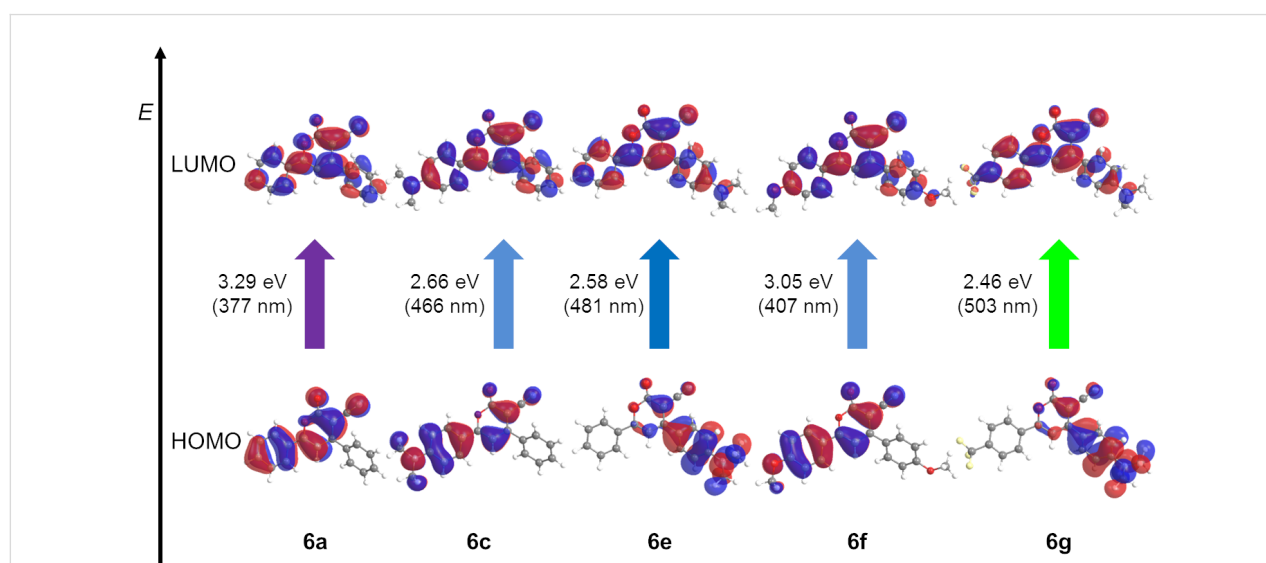


Figure 17: Selected DFT-computed (B3LYP 6-311G**) Kohn–Sham FMOs for *1H*-pyridines **6a**, **6c**, **6e**, **6f**, and **6g** and representing contributions of the longest wavelength Franck–Condon absorption bands.

(5 mL), and ethyl cyanoacetate (**4**, 2.31 g, 20.0 mmol) were added and the mixture was stirred at 75 °C for 16 h. After the addition of CH₂Cl₂ (5.00 mL) and NaOH/FeSO₄ solution (5.00 mL), the solution was extracted with CH₂Cl₂ (3 × 50.0 mL). The combined organic layers were dried (anhydrous MgSO₄) and the solvent was removed in vacuo. The residue was purified by flash chromatography on silica gel (*n*-hexane/EtOAc 12:1 to 5:1 to 0:1) and washed with hot ethanol (5 mL) to give compound **5d** (513 mg, 25%) as orange solid. Mp 223–233 °C; ¹H NMR (300 MHz, CDCl₃) δ 1.38 (t, *J* = 7.1 Hz, 3H), 4.30 (q, *J* = 7.1 Hz, 2H), 7.12 (dd, *J* = 1.5, 1.6 Hz, 1H), 7.44 (dd, *J* = 1.5, 1.6 Hz, 1H), 7.56–7.63 (m, 3H), 7.78–7.84 (m, 6H), 14.57 (s, 1H); ¹³C NMR (150 MHz, CDCl₃) δ 14.7 (CH₃), 60.6 (CH₂), 63.5 (C_{quat}), 109.2 (CH), 116.0 (CH), 119.5 (C_{quat}), 123.9 (q, *J*_{C-F} = 273 Hz, C_{quat}), 126.1 (CH), 126.2–126.7 (m, CH), 127.8 (CH), 130.1 (CH), 131.6 (CH), 132.3 (C_{quat}), 132.4 (q, *J*_{C-F} = 32.9 Hz, C_{quat}), 140.6 (C_{quat}), 146.6 (C_{quat}), 151.2 (C_{quat}), 156.0 (C_{quat}), 171.0 (C_{quat}); EIMS (70 eV, *m/z* (%)): 410 ([M]⁺, 24), 366 (24), 365 ([M – C₂H₅O]⁺, 100), 339 (12), 338 ([M – C₃H₅O₂]⁺, 53), 337 (38), 308 (8), 240 (23), 149 ([M – C₁₆H₁₂F₃]⁺, 11); IR (ATR) $\tilde{\nu}$ [cm⁻¹]: 3092 (w), 2992 (w), 2963 (w), 2943 (w), 2876 (w), 2806 (w), 2193 (m), 1625 (m), 1620 (m), 1597 (m), 1577 (m), 1506 (w), 1466 (w), 1413 (w), 1396 (w), 1369 (w), 1308 (m), 1300 (m), 1283 (s), 1258 (m), 1206 (w), 1165 (m), 1115 (s), 1092 (m), 1082 (m), 1071 (m), 1045 (s), 1030 (m), 1015 (m), 980 (m), 976 (m), 968 (w), 920 (w), 885 (w), 874 (w), 837 (s), 829 (m), 764 (s), 745 (w), 727 (w), 685 (m), 662 (w), 655 (w), 650 (w); UV–vis (CH₂Cl₂) λ_{\max} [nm] (ϵ [L·mol⁻¹·cm⁻¹]): 274 (32000), 321 (18100), 428 (10000); emission (CH₂Cl₂) λ_{\max} [nm] (Stokes shift [cm⁻¹]): 565 (5700); quantum yield (CH₂Cl₂) Φ_f : 0.01; Anal. calcd for C₂₃H₁₇F₃N₂O₂ (410.1): C, 67.31; H, 4.18; N, 6.83; found: C, 67.50; H, 4.32; N, 6.70.

Typical procedure for the cyclocondensation synthesis of compound **6c**

1-[4-(Dimethylamino)phenyl]-3-phenylprop-2-yn-1-one (**3c**, 249 mg, 1.00 mmol) was placed in a dry Schlenk tube and ethanol (2 mL) was added. Sodium carbonate (86.0 mg, 0.80 mmol), sodium acetate (50.0 mg, 0.60 mmol), water (1 mL), and ethyl cyanoacetate (**4**, 462 mg, 4.00 mmol) were added and the mixture was stirred at 75 °C for 16 h. After the addition of CH₂Cl₂ (5.00 mL) and NaOH/FeSO₄ solution (5.00 mL), the solution was extracted with CH₂Cl₂ (3 × 50.0 mL). The combined organic layers were dried (anhydrous MgSO₄) and the solvent was removed in vacuo. The residue was purified by flash chromatography on silica gel (*n*-hexane/EtOAc 5:1 to 1:1 to 0:1) and washed with hot ethanol (2.00 mL) and compound **6c** (37.0 mg, 12%) was obtained as deep purple solid. Mp 224–253 °C; ¹H NMR (300 MHz, CDCl₃) δ 3.10 (s, 6H), 6.69 (s, 1H), 6.69–6.75 (m, 2H),

7.51–7.58 (m, 3H), 7.67–7.73 (m, 2H), 7.78–7.85 (m, 2 H); ¹³C NMR (75 MHz, CDCl₃) δ 40.2 (CH₃), 91.1 (C_{quat}), 100.1 (CH), 111.8 (CH), 115.7 (C_{quat}), 116.5 (C_{quat}), 128.0 (CH), 128.8 (CH), 129.3 (CH), 131.6 (CH), 135.3 (C_{quat}), 153.4 (C_{quat}), 160.3 (C_{quat}), 164.1 (C_{quat}), 164.9 (C_{quat}). EIMS (70 eV, *m/z* (%)): 317 (15), 316 ([M]⁺, 66), 293 (11), 289 ([M – CN]⁺, 11), 288 ([M – CO]⁺, 51), 287 (19), 167 ([M – C₉H₁₁NO]⁺, 18), 150 (11), 149 ([M – C₁₁H₅NO]⁺, 100), 148 (20), 144 (13), 127 ([M – C₁₁H₁₁NO₂]⁺, 12), 85 (13), 71 (22), 57 (18), 43 ([M – C₁₈H₁₁NO₂]⁺, 13); IR (ATR) $\tilde{\nu}$ [cm⁻¹]: 3092 (w), 3048 (w), 2901 (w), 2864 (w), 2812 (w), 2739 (w), 2212 (w), 1708 (m), 1706 (m), 1609 (m), 1589 (m), 1570 (m), 1530 (m), 1497 (m), 1491 (m), 1482 (m), 1478 (m), 1473 (m), 1467 (m), 1458 (m), 1433 (m), 1375 (m), 1360 (m), 1333 (m), 1252 (m), 1209 (m), 1171 (m), 1159 (m), 1125 (m), 1111 (m), 1082 (m), 1059 (m), 1020 (m), 995 (m), 953 (m), 945 (m), 924 (w), 853 (m), 818 (s), 795 (m), 750 (m), 748 (m), 692 (s), 669 (m), 640 (m); UV–vis (CH₂Cl₂) λ_{\max} [nm] (ϵ [L·mol⁻¹·cm⁻¹]): 294 (18800), 482 (47300); emission (CH₂Cl₂) λ_{\max} [nm] (Stokes-shift [cm⁻¹]): 567 (3100); quantum yield (CH₂Cl₂) Φ_f : 0.99; emission (solid) λ_{\max} [nm]: 694; quantum yield (solid) Φ_f : 0.11; Anal. calcd for C₂₀H₁₆N₂O₂ (316.1): C, 75.93; H, 5.10; N, 8.86; found: C, 75.74; H, 5.19; N, 8.56.

Typical procedure for the cyclocondensation synthesis of compound **8a**

1,3-Diphenylprop-2-yn-1-one (**3a**, 103 mg, 0.50 mmol) was placed in a dry Schlenk tube and ethanol (1.00 mL) was added. Sodium carbonate (43.0 mg, 0.40 mmol), sodium acetate (25.0 mg, 0.30 mmol), water (50.0 μ L) and diethyl (*Z*)-3-amino-2-cyanopent-2-endoate (**7**, 226 mg, 1.00 mmol) were added and the mixture was stirred at 75 °C for 16 h. After the addition of CH₂Cl₂ (5.00 mL) and NaOH/FeSO₄ solution (5.00 mL), the solution was extracted with CH₂Cl₂ (3 × 50.0 mL). The combined organic layers were dried (anhydrous MgSO₄) and the solvent was removed in vacuo. The residue was purified by flash chromatography on silica gel (*n*-hexane/EtOAc 5:1 to 1:1 to 0:1) and washed with hot ethanol (5.00 mL) to furnish compound **8a** (108 mg, 52%) as yellow solid. Mp 140–146 °C; ¹H NMR (300 MHz, CDCl₃) δ 1.08 (t, *J* = 7.2 Hz, 3H), 1.37 (t, *J* = 7.1 Hz, 3H), 4.22 (q, *J* = 7.2 Hz, 2H), 4.31 (q, *J* = 7.1 Hz, 2H), 6.94 (d, *J* = 1.9 Hz, 1H), 7.40–7.48 (m, 5H), 7.55–7.62 (m, 3H), 7.75–7.84 (m, 2H), 15.60 (s, 1H); ¹³C NMR (75 MHz, CDCl₃) δ 13.7 (CH₃), 14.7 (CH₃), 60.9 (CH₂), 62.2 (CH₂), 62.7 (C_{quat}), 112.2 (CH), 118.2 (C_{quat}), 122.8 (C_{quat}), 126.3 (CH), 127.9 (CH), 128.8 (CH), 129.6 (CH), 130.1 (CH), 131.77 (CH), 131.84 (C_{quat}), 137.4 (C_{quat}), 146.1 (C_{quat}), 151.9 (C_{quat}), 153.0 (C_{quat}), 165.1 (C_{quat}), 172.1 (C_{quat}); EIMS (70 eV, *m/z* (%)): 415 ([M + H]⁺, 26), 414 ([M]⁺, 97), 369 ([M – C₂H₅O]⁺, 18), 342 (28), 341 ([M – C₃H₅O]⁺, 27), 340 ([M – C₃H₆O]⁺, 12), 314 (20), 313

([M – C₈H₅]⁺, 57), 298 (24), 297 ([M – C₅H₉O₃]⁺, 27), 296 ([M – C₅H₁₀O₃]⁺, 33), 287 (10), 286 (25), 271 (24), 270 ([M – C₆H₈O₄]⁺, 100), 269 (23), 268 ([M – C₆H₁₀O₄]⁺, 21), 266 (12), 258 ([M – C₇H₁₀NO₃]⁺, 14), 245 (18), 241 (13), 240 (26), 231 (15), 230 ([M – C₈H₁₀NO₄]⁺, 34), 203 (19), 202 (31), 164 (13); IR (ATR) $\tilde{\nu}$ [cm⁻¹]: 2978 (w), 2895 (w), 2197 (m), 1722 (m), 1636 (m), 1593 (s), 1578 (m), 1501 (m), 1489 (w), 1462 (w), 1441 (w), 1420 (w), 1364 (w), 1308 (m), 1288 (m), 1248 (s), 1188 (w), 1169 (m), 1134 (m), 1113 (s), 1092 (m), 1067 (m), 1047 (m), 1028 (w), 1001 (w), 885 (m), 854 (m), 847 (w), 775 (w), 758 (s), 746 (m), 694 (m), 658 (w); UV–vis (CH₂Cl₂) λ_{max} [nm] (ϵ [L·mol⁻¹·cm⁻¹]): 274 (20300), 324 (20100), 417 (7700); emission (CH₂Cl₂) λ_{max} [nm] (Stokes shift [cm⁻¹]): 557 (6000); quantum yield (CH₂Cl₂) $\Phi_{\text{f}} = < 0.01$; Anal. calcd for C₂₅H₂₂N₂O₄ (414.2): C, 72.45; H, 5.35; N, 6.76; found: C, 71.97; H, 5.45; N, 6.52.

Supporting Information

For experimental details of the synthesis and analytical data of compounds **3**, **5**, **6**, and **8**, ¹H and ¹³C NMR, and absorption and emission spectra of compounds **5**, **6**, and **8**, solid state emission spectra of compounds **5** and **6**, X-ray structural data of compound **5a**, and DFT/TDDFT calculations of compounds **5** and **6**, see below.

Supporting Information File 1

Additional experimental and calculated data.

[<https://www.beilstein-journals.org/bjoc/content/supplementary/1860-5397-15-262-S1.pdf>]

Acknowledgements

The authors gratefully acknowledge the Deutsche Forschungsgemeinschaft (DFG, Mu 1088-9/1) and the Fonds der Chemischen Industrie and also cordially thank Arno Schneeweis for measuring the quantum yield of compound **6c** in the solid state in cooperation with Hamamatsu Photonics Deutschland GmbH, Herrsching am Ammersee, Germany.

Statement

The reported results have been summarized in the inaugural dissertation "Diversitätsorientierte Synthese von Heterocyclen über Cyclokondensationen von Alkinonen und CH-aciden Estern" by Dr. Natascha Breuer, Heinrich Heine University Düsseldorf, 2018.

ORCID® iDs

Christoph Janiak - <https://orcid.org/0000-0002-6288-9605>

Thomas J. J. Müller - <https://orcid.org/0000-0001-9809-724X>

References

1. Yao, J.; Yang, M.; Duan, Y. *Chem. Rev.* **2014**, *114*, 6130–6178. doi:10.1021/cr200359p
2. Wysocki, L. M.; Lavis, L. D. *Curr. Opin. Chem. Biol.* **2011**, *15*, 752–759. doi:10.1016/j.cbpa.2011.10.013
3. Day, R. N.; Davidson, M. W. *Chem. Soc. Rev.* **2009**, *38*, 2887–2921. doi:10.1039/b901966a
4. Wegner, K. D.; Hildebrandt, N. *Chem. Soc. Rev.* **2015**, *44*, 4792–4834. doi:10.1039/c4cs00532e
5. Zhu, M.; Yang, C. *Chem. Soc. Rev.* **2013**, *42*, 4963–4976. doi:10.1039/c3cs35440g
6. Figueira-Duarte, T. M.; Müllen, K. *Chem. Rev.* **2011**, *111*, 7260–7314. doi:10.1021/cr100428a
7. Forrest, S. R.; Thompson, M. E. *Chem. Rev.* **2007**, *107*, 923–925. doi:10.1021/cr0501590
8. Grimsdale, A. C.; Leok Chan, K.; Martin, R. E.; Jokisz, P. G.; Holmes, A. B. *Chem. Rev.* **2009**, *109*, 897–1091. doi:10.1021/cr000013v
9. Kanibolotsky, A. L.; Perepichka, I. F.; Skabara, P. J. *Chem. Soc. Rev.* **2010**, *39*, 2695–2728. doi:10.1039/b918154g
10. Wang, X.; Zhang, F.; Liu, J.; Tang, R.; Fu, Y.; Wu, D.; Xu, Q.; Zhuang, X.; He, G.; Feng, X. *Org. Lett.* **2013**, *15*, 5714–5717. doi:10.1021/ol402745r
11. de Halleux, V.; Calbert, J.-P.; Brocorens, P.; Cornil, J.; Declercq, J.-P.; Brédas, J.-L.; Geerts, Y. *Adv. Funct. Mater.* **2004**, *14*, 649–659. doi:10.1002/adfm.200400006
12. Hassheider, T.; Benning, S. A.; Kitzerow, H.-S.; Achard, M.-F.; Bock, H. *Angew. Chem., Int. Ed.* **2001**, *40*, 2060–2063. doi:10.1002/1521-3773(20010601)40:11<2060::aid-anie2060>3.3.co;2-8
13. Kartha, K. K.; Babu, S. S.; Srinivasan, S.; Ajayaghosh, A. *J. Am. Chem. Soc.* **2012**, *134*, 4834–4841. doi:10.1021/ja210728c
14. Thimmarayaperumal, S.; Shanmugam, S. *ACS Omega* **2017**, *2*, 4900–4910. doi:10.1021/acsomega.7b00627
15. Park, S.-Y.; Ebihara, M.; Kubota, Y.; Funabiki, K.; Matsui, M. *Dyes Pigm.* **2009**, *82*, 258–267. doi:10.1016/j.dyepig.2009.01.014
16. Hagimori, M.; Mizuyama, N.; Yokota, K.; Nishimura, Y.; Suzuta, M.; Tai, C.-K.; Wang, B.-C.; Wang, S.-L.; Shih, T.-L.; Wu, K.-D.; Huang, Z.-S.; Tseng, S.-C.; Chen, C.-Y.; Lu, J.-W.; Wei, H.-H.; Kawashima, K.; Kawashima, S.; Tominaga, Y. *Dyes Pigm.* **2012**, *92*, 1069–1074. doi:10.1016/j.dyepig.2011.05.014
17. Levi, L.; Müller, T. J. J. *Chem. Soc. Rev.* **2016**, *45*, 2825–2846. doi:10.1039/c5cs00805k
18. Levi, L.; Müller, T. J. J. *Eur. J. Org. Chem.* **2016**, 2902–2918. doi:10.1002/ejoc.201600409
19. Müller, T. J. J. *Drug Discovery Today: Technol.* **2018**, *29*, 19–26. doi:10.1016/j.ddtec.2018.06.003
20. Merkt, F. K.; Müller, T. J. J. *Isr. J. Chem.* **2018**, *58*, 889–900. doi:10.1002/ijch.201800058
21. D'Souza, D. M.; Müller, T. J. J. *Chem. Soc. Rev.* **2007**, *36*, 1095–1108. doi:10.1039/b608235c
22. Gers-Panther, C. F.; Müller, T. J. J. *Adv. Heterocycl. Chem.* **2016**, *120*, 67–98. doi:10.1016/bs.aihch.2016.04.007
23. Breuer, N.; Müller, T. J. J. *Synthesis* **2018**, *50*, 2741–2752. doi:10.1055/s-0037-1610129
24. Tominaga, Y.; Mizuyama, N.; Murakami, Y.; Nagaoka, J.; Kohra, S.; Ueda, K.; Hiraoka, K.; Shigemitsu, Y. *Heterocycles* **2006**, *68*, 1105–1108. doi:10.3987/com-06-10741

25. Mizuyama, N.; Murakami, Y.; Nakatani, T.; Kuronita, K.; Kohra, S.; Ueda, K.; Hiraoka, K.; Tominaga, Y. *J. Heterocycl. Chem.* **2008**, *45*, 265–277. doi:10.1002/jhet.5570450133
26. Tominaga, Y.; Mizuyama, N.; Shigemitsu, Y.; Wang, B.-C. *Heterocycles* **2009**, *78*, 555–570. doi:10.3987/rev-08-642
27. Shankar, R.; Shukla, H.; Singh, U. S.; Thakur, V.; Hajela, K. *Synth. Commun.* **2011**, *41*, 2738–2746. doi:10.1080/00397911.2010.515350
28. Fouli, F. A.; Basyouni, M. N. *Acta Chim. Acad. Sci. Hung.* **1981**, *106*, 297–302.
29. Sadek, K. U.; Fahmy, S. M.; Mohareb, R. M.; Elnagdi, M. H. *J. Chem. Eng. Data* **1984**, *29*, 101–103. doi:10.1021/je00035a033
30. Takaya, H.; Naota, T.; Murahashi, S.-I. *J. Am. Chem. Soc.* **1998**, *120*, 4244–4245. doi:10.1021/ja974106e
31. Hammond, G. B.; Plevy, R. G.; Sampson, P.; Tatlow, J. C. *J. Fluorine Chem.* **1988**, *40*, 81–98. doi:10.1016/s0022-1139(00)83057-2
32. D'Souza, D. M.; Müller, T. J. *Nat. Protoc.* **2008**, *3*, 1660–1665. doi:10.1038/nprot.2008.152
33. Götzinger, A. C.; Müller, T. J. *J. Org. Biomol. Chem.* **2016**, *14*, 3498–3500. doi:10.1039/c6ob00483k
34. Karpov, A. S.; Müller, T. J. *J. Org. Lett.* **2003**, *5*, 3451–3454. doi:10.1021/ol035212q
35. CCDC 1944699 (5a) contains the supplementary crystallographic data (excluding structure factors) for this paper. These data are provided free of charge by The Cambridge Crystallographic Data Centre.
36. Desiraju, G. R.; Steiner, T. *The weak hydrogen bond. IUCr Monograph on Crystallography*; Oxford Science: Oxford, United Kingdom, 1999; Vol. 9.
37. Desiraju, G. R. *Acc. Chem. Res.* **2002**, *35*, 565–573. doi:10.1021/ar010054t
38. Janiak, C.; Scharmann, T. G. *Polyhedron* **2003**, *22*, 1123–1133. doi:10.1016/s0277-5387(03)00098-6
39. Shivakumar, K.; Vidyasagar, A.; Naidu, A.; Gonnade, R. G.; Sureshan, K. M. *CrystEngComm* **2012**, *14*, 519–524. doi:10.1039/c1ce05997a
40. Anelli, P. L.; Ashton, P. R.; Ballardini, R.; Balzani, V.; Delgado, M.; Gandolfi, M. T.; Goodnow, T. T.; Kaifer, A. E.; Philp, D. *J. Am. Chem. Soc.* **1992**, *114*, 193–218. doi:10.1021/ja00027a027
41. Janiak, C.; Temizdemir, S.; Dechert, S.; Deck, W.; Girgsdies, F.; Heinze, J.; Kolm, M.; Scharmann, T.; Zipffel, O. *Eur. J. Inorg. Chem.* **2000**, 1229–1241. doi:10.1002/(sici)1099-0682(200006)2000:6<1229::aid-ejic1229>3.3.co;2-g
42. N. Laxmi Madhavi, N.; R. Desiraju, G.; K. Katz, A.; L. Carrell, H.; Nangia, A. *Chem. Commun.* **1997**, 1953–1954. doi:10.1039/a705836e
43. Nishio, M. *CrystEngComm* **2004**, *6*, 130–158. doi:10.1039/b313104a
44. Nishio, M. *Phys. Chem. Chem. Phys.* **2011**, *13*, 13873–13900. doi:10.1039/c1cp20404a
45. Nishio, M.; Hirota, M.; Umezawa, Y. *The CH/π interaction (evidence, nature and consequences)*; Wiley-VCH: New York, NY, U.S.A., 1998.
46. Nishio, M.; Umezawa, Y.; Honda, K.; Tsuboyama, S.; Suezawa, H. *CrystEngComm* **2009**, *11*, 1757–1788. doi:10.1039/b902318f
47. Steiner, T.; Tamm, M.; Lutz, B.; Van Der Maas, J. *Chem. Commun.* **1996**, 1127–1128. doi:10.1039/cc9960001127
48. Umezawa, Y.; Tsuboyama, S.; Honda, K.; Uzawa, J.; Nishio, M. *Bull. Chem. Soc. Jpn.* **1998**, *71*, 1207–1213. doi:10.1246/bcsj.71.1207
49. Weiss, H.-C.; Bläser, D.; Boese, R.; Doughan, B. M.; Haley, M. M. *Chem. Commun.* **1997**, 1703–1704. doi:10.1039/a704070i
50. Janiak, C. *J. Chem. Soc., Dalton Trans.* **2000**, 3885–3896. doi:10.1039/b003010o
51. Janiak, C.; Uehlin, L.; Wu, H.-P.; Klüfers, P.; Piotrowski, H.; Scharmann, T. G. *J. Chem. Soc., Dalton Trans.* **1999**, 3121–3131. doi:10.1039/a904829d
52. Lozana, V.; Lassahn, P.-G.; Zhang, C.; Wu, B.; Janiak, C.; Rheinwald, G.; Lang, H. *Z. Naturforsch., B: J. Chem. Sci.* **2003**, *58*, 1152–1164. doi:10.1515/znb-2003-1202
53. Wu, H.-P.; Janiak, C.; Rheinwald, G.; Lang, H. *J. Chem. Soc., Dalton Trans.* **1999**, 183–190. doi:10.1039/a807450j
54. Wu, H.-P.; Janiak, C.; Uehlin, L.; Klüfers, P.; Mayer, P. *Chem. Commun.* **1998**, 2637–2638. doi:10.1039/a807522k
55. Yang, X.-J.; Drepper, F.; Wu, B.; Sun, W.-H.; Haehnel, W.; Janiak, C. *Dalton Trans.* **2005**, 256–267. doi:10.1039/b414999h
56. Zhang, C.; Janiak, C. *Z. Anorg. Allg. Chem.* **2001**, *627*, 1972–1975. doi:10.1002/1521-3749(200108)627:8<1972::aid-zaac1972>3.0.co;2-k
57. Zhang, C.; Janiak, C. *J. Chem. Crystallogr.* **2001**, *31*, 29–35. doi:10.1023/a:1013774502147
58. Rurack, K.; Spieles, M. *Anal. Chem. (Washington, DC, U. S.)* **2011**, *83*, 1232–1242. doi:10.1021/ac101329h
59. Lakowicz, J. R. *Principles of Fluorescence Spectroscopy*, 3rd ed.; Springer: Boston, MA, U.S.A., 2006. doi:10.1007/978-0-387-46312-4
60. Lippert, E. *Z. Elektrochem.* **1957**, 962–975.
61. Luo, J.; Song, K.; Gu, F. I.; Miao, Q. *Chem. Sci.* **2011**, *2*, 2029–2034. doi:10.1039/c1sc00340b
62. Mei, J.; Hong, Y.; Lam, J. W. Y.; Qin, A.; Tang, Y.; Tang, B. Z. *Adv. Mater. (Weinheim, Ger.)* **2014**, *26*, 5429–5479. doi:10.1002/adma.201401356
63. Müller, T. J. J. Multicomponent and Domino Syntheses of AIE Chromophores. In *Aggregation Induced Emission: Materials and Applications*, Fujiki, M.; Liu, B.; Tang, B. Z., Eds.; American Chemical Society: Washington, DC, U.S.A., 2016; pp 85–112. doi:10.1021/bk-2016-1226.ch006
64. Liu, B.; Tang, B. Z. *Chem. – Asian J.* **2019**, *14*, 672–673. doi:10.1002/asia.201900185
65. Becke, A. D. *J. Chem. Phys.* **1993**, *98*, 1372–1377. doi:10.1063/1.464304
66. Kim, K.; Jordan, K. D. *J. Phys. Chem.* **1994**, *98*, 10089–10094. doi:10.1021/j100091a024
67. Lee, C.; Yang, W.; Parr, R. G. *Phys. Rev. B* **1988**, *37*, 785–789. doi:10.1103/physrevb.37.785
68. Stephens, P. J.; Devlin, F. J.; Chabalowski, C. F.; Frisch, M. J. *J. Phys. Chem.* **1994**, *98*, 11623–11627. doi:10.1021/j100096a001
69. Krishnan, R.; Binkley, J. S.; Seeger, R.; Pople, J. A. *J. Chem. Phys.* **1980**, *72*, 650–654. doi:10.1063/1.438955
70. Scalmani, G.; Frisch, M. J. *J. Chem. Phys.* **2010**, *132*, 114110. doi:10.1063/1.3359469

License and Terms

This is an Open Access article under the terms of the Creative Commons Attribution License (<http://creativecommons.org/licenses/by/4.0>). Please note that the reuse, redistribution and reproduction in particular requires that the authors and source are credited.

The license is subject to the *Beilstein Journal of Organic Chemistry* terms and conditions: (<https://www.beilstein-journals.org/bjoc>)

The definitive version of this article is the electronic one which can be found at:
[doi:10.3762/bjoc.15.262](https://doi.org/10.3762/bjoc.15.262)